Electromagnetic response of a Gaussian beam to high-frequency relic gravitational waves in quintessential inflationary models

Fang-Yu Li*
Department of Physics, Chongqing University, Chongqing 400044, People's Republic of China

Meng-Xi Tang
Department of Physics, Zhongshan University, Guangzhou 510275, People's Republic of China

Dong-Ping Shi
Department of Physics, Chongqing University, Chongqing 400044, People's Republic of China
(Received 3 December 2002; published 19 May 2003)

The maximal signal and peak of high-frequency relic gravitational waves (GW's), recently predicted by quintessential inflationary models, may be firmly localized in the gigahertz region; the energy density of the relic gravitons in critical units (i.e., $h_0^2\Omega_{GW}$) is of the order of 10^{-6}, roughly eight orders of magnitude larger than in ordinary inflationary models. This is just the best frequency band for the electromagnetic (e.m.) response to high-frequency GW's in smaller e.m. detecting systems. We consider the e.m. response of a Gaussian beam passing through a static magnetic field to a high-frequency relic GW. It is found that under the synchroresonance condition the first-order perturbative e.m. power fluxes will contain a ''left circular wave'' and a ''right circular wave'' around the symmetrical axis of the Gaussian beam, but the perturbative effects produced by the states of + polarization and × polarization of the relic GW have different properties, and the perturbations of their behavior are obviously different from those of the background e.m. fields in the local regions. For a high-frequency relic GW with the typical parameters $\nu_g = 10^{10}$ Hz, $h = 10^{-30}$ in quintessential inflationary models, the corresponding perturbative photon flux passing through a region of 10^{-2} m^2 would be expected to be 10^3 s^{-1}. This is the largest perturbative photon flux we recently analyzed and estimated using the typical laboratory parameters. In addition, we also discuss the geometrical phase shift generated by high-frequency relic GW's in the Gaussian beam and estimate possible physical effects.

DOI: 10.1103/PhysRevD.67.104008 PACS number(s): 04.30.Nk, 04.25.Nx, 04.30.Db, 04.80.Nn

I. INTRODUCTION

Relic gravitational waves (GW's) are very important sources for information on the very early Universe; the physical behavior of the relic GW's expresses the states and evolution of the early Universe. Either direct detection or indirect tests of the relic GW's might provide new ways to observe our Universe. On the other hand, the expected properties of the relic GW's, such as amplitudes, polarizations, frequency band, energy densities, and spectra, etc., are dependent on the concrete universe model. Thus the expected features of the relic GW's and the concrete universe model have a closed relation. In recent years, quintessential inflationary models have been much discussed [1–5], and some astrophysical and cosmological observations seem to indicate [1,5,6] that these models are explicit and observationally acceptable. One important expectation [1,2] of the models is that the maximal signal and peak of the relic GW's are firmly localized in the GHz region, the corresponding energy density of the relic gravitons is almost eight orders of magnitude larger than in ordinary inflationary models, and the dimensionless amplitude of the relic GW's in the region can reach up to roughly 10^{-30} [1]. This is about five orders of magnitude more than that of the standing GW discussed in Refs. [7– 9]. Moreover, because the resonant frequencies between the GW's and e.m. fields in some smaller e.m. detection systems (e.g., microwave cavities, strong e.m. wave beams, and so on) [7–12], are distributed just right in the GHz region, the results offered new hopes for e.m. detection of the GW's. [Note that the frequency band detected by VIRGO [13], LIGO (Laser Interferometer Gravitational Wave Observatory) [14,15], and LISA (Laser Interferometer Space Antenna) [16] are often distributed in the region of $10^{-4}-10^{4}$ Hz (which is also the most promising detection frequency band for the usual astronomical GW's); thus the e.m. response to the high-frequency relic GW's might provide a new detection window in the GHz band.]

In this paper, we shall study the e.m. response to a high-frequency relic GW by a Gaussian beam propagating through a static magnetic field. We consider it for the following reasons. (1) Unlike the usual e.m. response to GW's by an ideal planar e.m. wave [17], the Gaussian beam is a realized e.m. wave beam satisfying physical boundary conditions, and because of the special properties of the Gaussian function of the beam, the resonant response of the Gaussian beam to high-frequency GW's has better space accumulation effects (see Fig. 5 below) than that of a plane EM wave (see Fig. 7 in Ref. [8]). (2) In recent years, strong and ultrastrong lasers and microwave beams have been generated [18–21] under laboratory conditions, many of the beams have Gaussian-type or quasi-Gaussian-type distributions, and they usually have good monochromaticity in the GHz region. (3) The e.m. response in the GHz band means that the dimensions of the

*Email address: cqufangyuli@hotmail.com

e.m. system may be reduced to the typical laboratory size (e.g., the magnitude of a meter); thus the requirements on other parameters can be further relaxed. (4) Unlike the cavity electrodynamical response to GW's (in general, the detecting cavities are closed systems for the normal e.m. modes stored inside the cavities), a Gaussian beam propagating through a static e.m. field is an open system. In this case, the e.m. perturbations might have a more direct displaying effect, although they have no energy accumulation effect in the cavity electrodynamical response. Therefore, the e.m. response of Gaussian beams to GW's and the e.m. detection of microwave cavities of GW's have very strong complementarity for each other; this is also one of the motivations for this investigation.

The basic plan of this paper is the following. In Sec. II we present the usual form of the Gaussian beam in flat space-time. In Sec. III we consider the e.m. response of a Gaussian beam passing through a static magnetic field to high-frequency relic GW's in the quintessential inflationary models. It includes perturbation solutions of the electrodynamical equations in curved space-time, the first-order perturbative e.m. power fluxes (or in quantum language the perturbative photon fluxes). Moreover, we give numerical estimations of our results. In Sec. IV we discuss the possible geometrical phase shift produced by high-frequency relic GW's. Our conclusions are summarized in Sec. V.

II. A GAUSSIAN BEAM IN FLAT SPACE-TIME

It is well known that in flat space-time (i.e., when GW's are absent) the usual form of the fundamental Gaussian beam is [22]

$$\psi=\frac{\psi_0}{\sqrt{1+(z/f)^2}}\exp\left(-\frac{r^2}{W^2}\right)\exp\left\{i\left[(k_e z-\omega_e t)-\tan^{-1}\frac{z}{f}+\frac{k_e r}{2R}+\delta\right]\right\}, \tag{1}$$

where $r^2=x^2+y^2$, $k_e=2\pi/\lambda_e$, $f=\pi W_0^2/\lambda_e$, $W=W_0[1+(z/f)^2]^{1/2}$, and $R=z+f^2/z$. ψ_0 is the maximal amplitude of the electric (or magnetic) field of the Gaussian beam, i.e., the amplitude at the plane $z=0$, W_0 is the minimum spot size, namely, the spot radius at the plane $z=0$, and δ is an arbitrary phase factor. ψ satisfies the scalar Helmholtz equation

$$\nabla^2\psi+k_e^2\psi=0. \tag{2}$$

For a Gaussian beam in vacuum, we have $k_e^2=\omega_e^2\mu_0\epsilon_0$, where ω_e is the angular frequency of the Gaussian beam.

Supposing that the electric field of the Gaussian beam is pointed along the direction of the x axis, that it is expressed as Eq. (1), and that a static magnetic field pointing along the y axis is localized in the region $-l/2\leqslant z\leqslant l/2$, then we have

$$E^{(0)}=\tilde{E}_x{}^{(0)}=\psi,\quad E_y^{(0)}=E_z^{(0)}=0,$$

$$B^{(0)}=\hat{B}^{(0)}=\begin{cases}\hat{B}_y^{(0)} & (-l/2\leqslant z\leqslant l/2),\\ 0 & (z\leqslant -l/2 \text{ and } z\geqslant l/2),\end{cases} \tag{3}$$

where the superscript 0 denotes the background e.m. fields, and the tilde and caret stand for the time-dependent and static fields, respectively. Using (we use mks units)

$$\tilde{\mathbf{B}}^{(0)}=-\frac{i}{\omega_e}\nabla\times\tilde{\mathbf{E}}^{(0)}, \tag{4}$$

and Eqs. (1) and (3), we obtain the time-dependent e.m. field components in cylindrical polar coordinates as follows:

$$\tilde{E}_r^{(0)}=\psi\cos\phi,\quad \tilde{E}_\phi^{(0)}=-\psi\sin\phi,\quad \tilde{E}_z^{(0)}=0, \tag{5}$$

$$\tilde{B}_r^{(0)}=-\frac{i}{\omega_e}\frac{\partial\psi}{\partial z}\sin\phi=\left\{\frac{\psi_0\sin\phi}{\omega_e[1+(z/f)^2]^{1/2}}\left[k_e+\frac{k_e r^2(f^2-z^2)}{2(f^2+z^2)^2}-\frac{f}{f^2+z^2}\right]+\frac{i\psi_0 z\sin\phi}{\omega_e f^2[1+(z/f)^2]^{3/2}}\left[1-\frac{2r^2}{W_0^2[1+(z/f)^2]}\right]\right\}$$
$$\times\exp\left(-\frac{r^2}{W^2}\right)\exp\left\{i\left[(k_e z-\omega_e t)-\tan^{-1}\frac{z}{f}+\frac{k_e r^2}{2R}+\delta\right]\right\}, \tag{6}$$

$$\tilde{B}_\phi^{(0)}=-\frac{i}{\omega_e}\frac{\partial\psi}{\partial z}\cos\phi$$
$$=\left\{\frac{\psi_0\cos\phi}{\omega_e[1+(z/f)^2]^{1/2}}\left[k_e+\frac{k_e r^2(f^2-z^2)}{2(f^2+z^2)^2}-\frac{f}{f^2+z^2}\right]+\frac{i\psi_0 z\cos\phi}{\omega_e f^2[1+(z/f)^2]^{3/2}}\left[1-\frac{2r^2}{W_0^2[1+(z/f)^2]}\right]\right\}$$
$$\times\exp\left(-\frac{r^2}{W^2}\right)\exp\left\{i\left[(k_e z-\omega_e t)-\tan^{-1}\frac{z}{f}+\frac{k_e r^2}{2R}+\delta\right]\right\}, \tag{7}$$

$$\tilde{B}_z^{(0)} = \frac{i}{\omega_e}\frac{\partial \psi}{\partial y}$$

$$= -\left\{\frac{\psi_0 k_e r\ \sin\ \phi}{\omega_e[1+(z/f)^2]^{1/2}(z+f^2/z)} + \frac{i2\psi_0 r\ \sin\ \phi}{\omega_e W_0^2[1+(z/f)^2]^{3/2}}\right\}\exp\left(-\frac{r^2}{W^2}\right)\exp\left\{i\left[(k_e z-\omega_e t)-\tan^{-1}\frac{z}{f}+\frac{k_e r^2}{2R}+\delta\right]\right\}. \quad (8)$$

With the help of Eq. (1) and Eqs. (5)–(8), we can calculate the power flux density of the Gaussian in flat space-time. For high-frequency e.m. power fluxes, only the nonvanishing average values of these with respect to time have an observable effect. From Eqs. (1) and (5)–(8), one finds

$$\overset{(0)}{\langle S^z\rangle} = \frac{1}{\mu_0}\langle \tilde{E}_x^{(0)}\tilde{B}_y^{(0)}\rangle$$

$$= \frac{\psi_0^2}{2\mu_0\omega_e[1+(z/f)^2]}\left[k_e + \frac{k_e r^2(f^2-z^2)}{2(f^2+z^2)^2} - \frac{f}{f^2+z^2}\right]\exp\left(-\frac{2r^2}{W^2}\right), \quad (9)$$

$$\overset{(0)}{\langle S^r\rangle} = \frac{1}{\mu_0}\langle \tilde{E}_\phi^{(0)}\tilde{B}_z^{(0)}\rangle$$

$$= \frac{\psi_0^2 k_e r\ \sin^2\ \phi}{2\mu_0\omega_e[1+(z/f)^2](z+f^2/z)}\exp\left(-\frac{2r^2}{W^2}\right), \quad (10)$$

$$\overset{(0)}{\langle S^\phi\rangle} = -\frac{1}{\mu_0}\langle \tilde{E}_r^{(0)}\tilde{B}_z^{(0)}\rangle$$

$$= \frac{\psi_0^2 k_e r\ \sin(2\phi)}{4\mu_0\omega_e[1+(z/f)^2](z+f^2/z)}\exp\left(-\frac{2r^2}{W^2}\right), \quad (11)$$

where $\overset{(0)}{\langle S^z\rangle}$, $\overset{(0)}{\langle S^r\rangle}$, and $\overset{(0)}{\langle S^\phi\rangle}$ represent the average values of the axial, radial, and tangential e.m. power flux densities, respectively; the angular brackets denote the average values with respect to time. We can see from Eqs. (9)–(11) that $\overset{(0)}{\langle S^r\rangle}_{z=0} = \overset{(0)}{\langle S^\phi\rangle}_{z=0} \equiv 0$, $\overset{(0)}{\langle S^z\rangle}_{z=0} = \overset{(0)}{\langle S^z\rangle}_{max}$, and $|\overset{(0)}{\langle S^z\rangle}| \gg |\overset{(0)}{\langle S^r\rangle}|$ and $|\overset{(0)}{\langle S^\phi\rangle}|$ in the region near the minimum spot. Thus, the propagation direction of the Gaussian beam is exactly parallel to the z axis only in the plane $z=0$. In the region of $z\neq 0$, because of the nonvanishing $\overset{(0)}{\langle S^r\rangle}$ and $\overset{(0)}{\langle S^\phi\rangle}$, the Gaussian beam will be asymptotically spread as $|z|$ increases.

We will show that when the GW is present, the Gaussian beam will be perturbed by the GW. In particular, under the synchroresonant condition (i.e., when the frequency $\omega_g/2\pi$ of the GW equals $\omega_e/2\pi$ of the Gaussian beam), nonvanishing first-order perturbative e.m. power fluxes can be produced, and their behavior is obviously different from that of the background e.m. fields in the local regions.

III. ELECTROMAGNETIC RESPONSE OF THE GAUSSIAN BEAM TO A HIGH-FREQUENCY RELIC GRAVITATIONAL WAVE

A. The high-frequency relic GW's in quintessential inflationary models

For the relic graviton spectrum in quintessential inflationary models, recent analyses [1,2] seem to indicate that, unlike in ordinary inflationary models, the maximum signal and peak are firmly localized in the GHz region, the corresponding energy density of the relic gravitons is almost eight orders of magnitude larger than that in ordinary inflationary models, and the dimensionless amplitude of the relic GW's in the GHz band can reach up to roughly 10^{-30} [1]. Thus smaller e.m. detection systems (not necessarily interferometers) may be suitable for the purpose of detecting high-frequency relic GW's.

In Fig. 1 one illustrates the relic graviton logarithmic energy spectra expected for typical ordinary inflationary models (curve I) and for quintessential inflationary models (curve II), respectively. The regions (1), (2), (3), (4)-1, (4)-2, (5), and (6) represent the detection frequency bands for LISA [16], LIGO [14,15], resonant-mass detectors [23–25], superconducting microwave cavities [10,11,38–40], Gaussian beams tuned to the GHz frequency band, and mini-ASTROD (miniastrodynamical space test of relativity using optical devices) [26], respectively. Presently operating mass detectors include ALLEGEO [23], EXPLORER [24], AURIGA, and NAUTILUS [25]. These detectors are often operating in the kHz frequency band. For example, the operating frequency of the cryogenic resonant-mass detector EXPLORER is 923 Hz [24]. Their sensitivity would be expected to be $\delta h \sim 10^{-19}$–10^{-22} roughly for GW's in the kHz band.

Giovannini [1] analyzed the relic GW's in quintessential inflationary models within the framework of quantum theory. In this framework the Fourier expansion of the field operators of the relic GW's can be written as

$$\hat{\mu}_\oplus(\vec{x},\eta) = \frac{1}{(2\pi)^{3/2}}\int d^3k_g[\hat{\mu}_\oplus(k_g,\eta)e^{i\vec{k}_g\cdot\vec{x}} + \hat{\mu}_\oplus^*(k_g,\eta)e^{-i\vec{k}_g\cdot\vec{x}}],$$

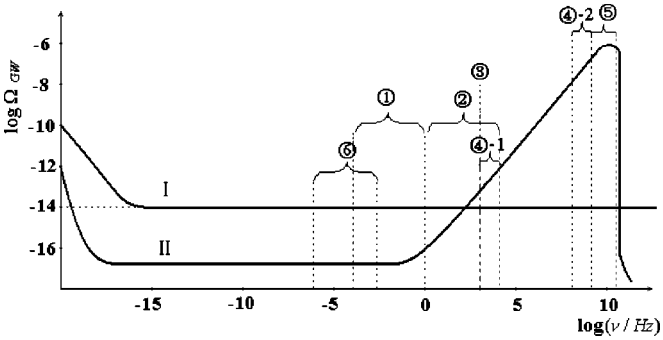

FIG. 1. Curves I and II represent the relic graviton logarithmic energy spectra (in critical units) expected in the usual ordinary inflationary models and in the quintessential inflationary models, respectively. The curves are taken from Ref. [1]. Here we illustrate roughly the distribution for some detection frequency bands. Region (1) expresses the detection frequency band of LISA ($\sim 10^{-4}$–1 Hz); region (2) is that of LIGO (~ 1–10^4 Hz); region (3)is that of the resonant-mass detectors ($\sim 10^3$ Hz); region (4)-1 is that of the difference-frequency resonant response of a microwave cavity ($\sim 10^3$–10^4 Hz), region (4)-2 ($\sim 10^8-10^9$ Hz) is that of the fundamental resonant response of a microwave cavity; region (5) is that of the Gaussian beams ($\sim 10^9$–10^{11} Hz); and region (6) is that of mini-ASTROD ($\sim 10^{-6}$–10^{-3} Hz). It can be seen that region (4)-2 coincides partly with the maximal signal and peak of the relic graviton energy spectra expected in quintessential inflationary models; the detection frequency band (5) of the Gaussian beam tuned to the GHz frequency region can be almost completely localized in this peak value region. For the relevant background in Fig. 1, we present a brief introduction in the Appendixes. (Appendix A: The cavity electromagnetic response to GW's. Appendix B: The dimensionless amplitude h and the power spectrum S_h of the relic GW's. Appendix C: ASTROD. Appendix D: Noise problems.)

$$\hat{\mu}_{\otimes}(\vec{x},\eta)=\frac{1}{(2\pi)^{3/2}}\int d^3k_g[\hat{\mu}_{\otimes}(k_g,\eta)e^{i\vec{k}_g\cdot\vec{x}} + \hat{\mu}^{*}_{\otimes}(k_g,\eta)e^{-i\vec{k}_g\cdot\vec{x}}], \tag{12}$$

where

$$\hat{\mu}_{\oplus}(k_g,\eta)=\psi_{\oplus}(k_g,\eta)\hat{a}_{\oplus}(k_g),$$

$$\hat{\mu}_{\otimes}(k_g,\eta)=\psi_{\otimes}(k_g,\eta)\hat{a}_{\otimes}(k_g), \tag{13}$$

$\oplus$ and $\otimes$ denote the $+$ and $\times$ polarization of the GW's, respectively, η is the conformal time, and $\hat{a}^{*}_{\oplus}$, $\hat{a}_{\oplus}$ and $\hat{a}^{*}_{\otimes}$, $\hat{a}_{\otimes}$ represent the creation and annihilation operators of the above two physical polarization states. From the viewpoint of observation, the classical picture of Eq. (12) corresponds to the amplitudes of the relic GW's with the two states of polarization, namely,

$$h_{\oplus}(\vec{x},\eta)=\frac{1}{(2\pi)^{3/2}}\int d^3k_g h_{\oplus}(k_g,\eta)e^{i\vec{k}_g\cdot\vec{x}},$$

$$h_{\otimes}(\vec{x},\eta)=\frac{1}{(2\pi)^{3/2}}\int d^3k_g h_{\otimes}(k_g,\eta)e^{i\vec{k}_g\cdot\vec{x}}, \tag{14}$$

where the integration spreads over the whole frequency band of the relic GW's. However, if we hope to realize the resonant response of a monochromatic Gaussian beam to the relic GW's, it is necessary to let the frequency of the Gaussian beam equal a certain frequency in the peak value region of the relic GW's (i.e., $\omega_e=\omega_g$). Fortunately, most strong microwave beams (including the Gaussian beam) generated by present technology are monochromatic or quasimonochromatic; thus a relic GW resonant with the Gaussian beam need be only one monochromatic component satisfying the condition $\omega_g=\omega_e$ in the relic GW frequency band. In this case the corresponding treatment can be greatly simplified without excluding the essential physical features. Of course, for the resonant response to the relic GW's on the earth, we should use the intervals of laboratory time [i.e., $cdt=a(\eta)d\eta$] and laboratory frequency [27]. Consequently, a monochromatic circular polarized plane relic GW propagating along the z axis can be written as

$$h_{\oplus}=h_{xx}=-h_{yy}=A_{\oplus}\exp(ik_{\alpha}x^{\alpha})=A_{\oplus}\exp[i(k_gz-\omega_gt)],$$

$$h_{\otimes}=h_{xy}=h_{yx}=iA_{\otimes}\exp(ik_{\alpha}x^{\alpha})=iA_{\otimes}\exp[i(k_gz-\omega_gt)]. \tag{15}$$

This is just the usual form of the GW in the TT gauge. Equation (15) can be viewed as the classical approximation of Eqs. (12) and (13) under the monochromatic wave condition.

Since the relic GW's in the peak value region of the quintessential inflationary models have very high frequency (the GHz frequency band), future measurements through microwave cavities or strong Gaussian beams may be useful. In particular, for the high-frequency relic GW's of 10^9 Hz $\leqslant\nu_g\leqslant 10^{11}$ Hz (these are the best peak frequency band expected in the quintessential inflationary models), using the e.m. response of the Gaussian beam would be more suitable (see Fig. 1).

B. The electromagnetic system in the high-frequency relic gravitational wavefield

From Eq. (15), the nonvanishing components of the metric tensor in Cartesian coordinates are given by

$$g_{00}=-1,\quad g_{11}=g_{xx}=1+h_{xx}=1+h_{\oplus},$$

$$g_{22}=g_{yy}=1+h_{yy}=1-h_{\oplus},$$

$$g_{12}=g_{21}=g_{xy}=g_{yx}=h_{xy}=h_{\otimes},\quad g_{33}=g_{zz}=1,$$

$$g^{00}=-1,\quad g^{11}=g^{xx}=1-h^{xx}=1-h_{\oplus},$$

$$g^{22}=g^{yy}=1-h^{yy}=1+h_{\oplus},$$

$$g^{12}=g^{21}=g^{xy}=g^{yx}=-h^{xy}=-h_{\otimes},\quad g^{33}=g^{zz}=1. \tag{16}$$

With the help of Eqs. (3)–(8) and considering the perturbation produced by the weak GW field expressed as Eqs. (15) and (16), the components of the e.m. field tensor in Cartesian coordinates can be written as

$$F_{01}=\tilde{F}_{01}^{(0)}+\tilde{F}_{01}^{(1)}=\frac{1}{c}(\tilde{E}_x^{(0)}+\tilde{E}_x^{(1)})=\frac{1}{c}(\psi+\tilde{E}_x^{(1)}),$$

$$F_{02}=\tilde{F}_{02}^{(1)}=\frac{1}{c}\tilde{E}_y^{(1)}, \quad F_{03}=\tilde{F}_{03}^{(1)}=\frac{1}{c}\tilde{E}_z^{(1)},$$

$$F_{12}=\tilde{F}_{12}^{(0)}+\tilde{F}_{12}^{(1)}=-(\tilde{B}_z^{(0)}+\tilde{B}_z^{(1)})=-\left(\frac{i}{\omega}\frac{\partial\psi}{\partial y}+\tilde{B}_z^{(1)}\right),$$

$$F_{13}=\hat{F}_{13}^{(0)}+\tilde{F}_{13}^{(0)}+\tilde{F}_{13}^{(1)}=\hat{B}_y^{(0)}+\tilde{B}_y^{(0)}+\tilde{B}_y^{(1)}$$
$$=\hat{B}_y^{(0)}-\frac{i}{\omega}\frac{\partial\psi}{\partial z}+\tilde{B}_y^{(1)},$$

$$F_{23}=\tilde{F}_{23}^{(1)}=\tilde{B}_x^{(1)}, \tag{17}$$

where $\hat{F}_{\mu\nu}^{(0)}$ and $\tilde{F}_{\mu\nu}^{(0)}$ represent the background static magnetic field $\hat{B}_y^{(0)}$ and the background e.m. wavefield (the Gaussian beam), respectively, and $\tilde{F}_{\mu\nu}^{(1)}$ is the first-order perturbation to the background e.m. field in the presence of the GW. For nonvanishing $F_{\mu\nu}^{(0)}$ and $F_{\mu\nu}^{(1)}$, we have $|\tilde{F}_{\mu\nu}^{(1)}| \ll |F_{\mu\nu}^{(0)}|$.

The e.m. response to the GW can be described by Maxwell equations in curved space-time, i.e.,

$$\frac{1}{\sqrt{-g}}\frac{\partial}{\partial x^\nu}(\sqrt{-g}\, g^{\mu\alpha}g^{\nu\beta}F_{\alpha\beta})=\mu_0 J^\mu, \tag{18}$$

$$F_{[\mu\nu,\alpha]}=0, \tag{19}$$

where J^μ indicates the four-dimensional electric current density. For the e.m. response in vacuum, because it has neither a real four-dimensional electric current nor the equivalent electric current caused by energy dissipation, such as Ohmic losses in the cavity electrodynamical response or dielectric losses [10], $J^\mu=0$ in Eq. (18).

Unlike the interaction of a plane e.m. wave with a plane GW (according to the Einstein-Maxwell equations under the condition of a weak gravitational field, if both the plane GW and plane e.m. wave have the same propagation direction, then the perturbation by the GW of the e.m. wave vanishes [17]), the electric and magnetic fields of the Gaussian beam are nonsymmetric [see Eqs. (1) and (5)–(8)]. In this case, using Eqs. (5)–(8) and (18),(19), it can be shown that even for a plane GW propagating along the positive z direction, it can produce a nonvanishing perturbative effect on the Gaussian beam. In order to find the concrete form of the perturbation produced by the direct interaction of the GW with the Gaussian beam, it is necessary to solve Eqs. (18) and (19) by substituting Eqs. (1), (5)–(8), (15), (16), and (17) into them, which is often quite difficult. However, as shown in Refs. [8,17,28,29], the orders of the amplitudes of the first-order perturbative electric and magnetic fields produced by the direct interaction of the GW with the e.m. wave (e.g., plane wave or Gaussian beam) are approximately $h\tilde{B}^{(0)}c$ and $h\tilde{B}^{(0)}$, respectively, while those generated by the direct interaction of the GW with the static magnetic field are approximately $h\hat{B}^{(0)}c$ and $h\hat{B}^{(0)}$, respectively. Thus corresponding amplitude ratio is about $h\tilde{B}^{(0)}/h\hat{B}^{(0)}$. In our case, we have chosen $\tilde{B}^{(0)}\sim 10^{-3}$ T, $\hat{B}^{(0)}\sim 10$ T, i.e., their ratio is only roughly 10^{-4}. Therefore, the former can be neglected. In other words, the contribution of the Gaussian beam is mainly expressed in the coherent synchroresonance (i.e., $\omega_e=\omega_g$) of it with the first-order perturbation $\tilde{F}_{\mu\nu}^{(1)}$ generated by the direct interaction of the GW with the static field $\hat{B}_y^{(0)}$. In this case, the process of solving Eqs. (18) and (19) can be greatly simplified, i.e., the static magnetic field $\hat{B}^{(0)}=\hat{B}_y^{(0)}$ can be seen as the unique background e.m. field in Eqs. (18) and (19). Under these circumstances, first we can solve Eqs. (18) and (19) in region II ($-l/2\leqslant z\leqslant l/2$, $\hat{B}^{(0)}=\hat{B}_y^{(0)}$) to find the first-order perturbation solutions; and second, using the boundary conditions one can obtain the first-order perturbation solutions in region I ($z\leqslant -l/2$, $\hat{B}^{(0)}=0$) and region III ($z\geqslant l/2$, $\hat{B}^{(0)}=0$).

Introducing Eqs. (15)–(17) into Eqs. (18),(19), and neglecting high-order infinitely small quantities and the perturbative effect produced by the direct interaction of the GW with the Gaussian beam, Eqs. (18) and (19) are reduced to

$$\frac{1}{c^2}\tilde{E}_{x,t}^{(1)}+\tilde{B}_{y,z}^{(1)}=\hat{B}_y^{(0)}h_{xx,z},$$

$$\tilde{E}_{x,z}^{(1)}+\tilde{B}_{y,t}^{(1)}=0, \tag{20}$$

$$\frac{1}{c^2}\tilde{E}_{y,t}^{(1)}+\tilde{B}_{x,z}^{(1)}=\hat{B}_y^{(0)}h_{xy,z},$$

$$\tilde{E}_{y,z}^{(1)}-\tilde{B}_{x,t}^{(1)}=0, \tag{21}$$

and

$$\tilde{E}_{z,t}^{(1)}=\tilde{E}_{z,z}^{(1)}=0, \quad \tilde{B}_{z,t}^{(1)}=\tilde{B}_{z,z}^{(1)}=0, \tag{22}$$

where the commas in the subscripts denote partial derivatives. Using Eq. (15), Eqs. (20)–(22) can also be expressed as the following inhomogeneous hyperbolic-type equations, respectively:

$$\Box\tilde{E}_x^{(1)}=\tilde{E}_{x,zz}^{(1)}-\frac{1}{c^2}\tilde{E}_{x,tt}^{(1)}=-A_\oplus\hat{B}_y^{(0)}k_g^2 c\, \exp[i(k_g z-\omega_g t)],$$

$$\Box\tilde{B}_y^{(1)}=\tilde{B}_{y,zz}^{(1)}-\frac{1}{c^2}\tilde{B}_{y,tt}^{(1)}=-A_\oplus\hat{B}_y^{(0)}k_g^2 \exp[i(k_g z-\omega_g t)], \tag{23}$$

$$\Box\tilde{E}_y^{(1)}=\tilde{E}_{y,zz}^{(1)}-\frac{1}{c^2}\tilde{E}_{y,tt}^{(1)}=-iA_{\otimes}\hat{B}_y^{(0)}k_g^2\ c\ \ \exp[i(k_gz-\omega_gt)],$$

$$\Box\tilde{B}_x^{(1)}=\tilde{B}_{x,zz}^{(1)}-\frac{1}{c^2}\tilde{B}_{x,tt}^{(1)}=iA_{\otimes}\hat{B}_y^{(0)}k_g^2\ \exp[i(k_gz-\omega_gt)], \tag{24}$$

$$\Box\tilde{E}_z^{(1)}=\Box\tilde{B}_z^{(1)}=0, \tag{25}$$

where $\Box$ indicates the d'Alembertian. Obviously, every solution of Eq. (20) must satisfy Eq. (23), and every solution of Eq. (21) must satisfy Eq. (24), and it is easily seen from Eqs. (22) and (25) that a physically reasonable solution of them is only

$$\tilde{E}_z^{(1)}=\tilde{B}_z^{(1)}=0. \tag{26}$$

The general solutions of Eqs. (20)–(24) in region II ($-l/2\leqslant z\leqslant l/2$) are given by

$$\begin{aligned}\tilde{E}_x^{(1)}&=\frac{i}{2}A_{\oplus}\hat{B}_y^{(0)}k_gc(z+l/2)\exp[i(k_gz-\omega_gt)]\\&\quad+b_1\ \exp[i(k_gz-\omega_gt)]+c_1\ \exp[i(k_gz+\omega_gt)],\\\tilde{B}_y^{(1)}&=\frac{i}{2}A_{\oplus}\hat{B}_y^{(0)}k_g(z+l/2)\exp[i(k_gz-\omega_gt)]\\&\quad+b_2\ \exp[i(k_gz-\omega_gt)]+c_2\ \exp[i(k_gz+\omega_gt)],\end{aligned} \tag{27}$$

$$\begin{aligned}\tilde{E}_y^{(1)}&=-\frac{1}{2}A_{\otimes}\hat{B}_y^{(0)}k_gc(z+l/2)\exp[i(k_gz-\omega_gt)]\\&\quad+ib_3\ \exp[i(k_gz-\omega_gt)]+ic_3\ \exp[i(k_gz+\omega_gt)],\\\tilde{B}_x^{(1)}&=\frac{1}{2}A_{\otimes}\hat{B}_y^{(0)}k_g(z+l/2)\exp[i(k_gz-\omega_gt)]\\&\quad+ib_4\ \exp[i(k_gz-\omega_gt)]+ic_4\ \exp[i(k_gz+\omega_gt)].\end{aligned} \tag{28}$$

The solutions, Eqs. (26), (27), and (28), show that perturbative e.m. waves produced by a plane GW satisfying the TT gauge must be transverse waves, and the background static magnetic field is perpendicular to the propagation direction of the GW. The constants in Eqs. (27) and (28) satisfy

$$\begin{aligned}b_1-cb_2&=-\frac{1}{2}A_{\oplus}\hat{B}_y^{(0)}c,\quad c_1+cc_2=0,\\b_3+cb_4&=-\frac{1}{2}A_{\otimes}\hat{B}_y^{(0)}c,\quad c_3-cc_4=0;\end{aligned} \tag{29}$$

their concrete forms will be defined by the physical requirements and boundary conditions.

The solutions (26)–(28) have similar features to those found by a number of authors [28,29] previously, but as we shall show, unlike previous work, our e.m. system is a possible scheme to display the first-order e.m. perturbations produced by the high-frequency relic GW's (GHz region) inside a typical laboratory size detector (not necessarily interferometers or e.m. cavities with giant dimensions); a particularly interesting feature of the first-order perturbation is the perturbative effect in some special directions and some special regions.

It should be pointed out that in curved space-time only local measurements made by an observer traveling in his world-line have definite observable meaning. These observable quantities are just the projections of the physical quantities as a tensor on tetrads of the observer's world-line. The tetrads consist of three spacelike mutually orthogonal vectors and a timelike vector directed along the four-velocity of the observer; the latter is perpendicular to the former. We indicate these with $\tau_{(\alpha)}^{\mu}$, where the index in parentheses numbers the vectors and the other refers to the components of the tetrads in the chosen coordinates. Consequently, the quantities $F_{(\alpha\beta)}$ measured by the observer are the tetrad components of the e.m. field tensor, that is,

$$F_{(\alpha\beta)}=F_{\mu\nu}\tau_{(\alpha)}^{\mu}\tau_{(\beta)}^{\nu}. \tag{30}$$

Obviously, for our e.m. system, the observer should be at rest in the static magnetic field, i.e., only the zeroth component of the four-velocity is nonvanishing. Thus, the tetrad $\tau_{(0)}^{\mu}$ has the form

$$\tau_{(0)}^{\mu}=(\tau_{(0)}^{0},0,0,0). \tag{31}$$

Using Eq. (16) and the orthonormality of the tetrads $g_{\mu\nu}\tau_{(\alpha)}^{\mu}\tau_{(\beta)}^{\nu}=\eta_{\alpha\beta}$, neglecting high-order infinitely small quantities, it is always possible to get

$$\begin{aligned}\tau_{(0)}^{\mu}&=(1,0,0,0),\\\tau_{(1)}^{\mu}&=\left(0,1-\frac{1}{2}h_{\oplus},0,0\right),\\\tau_{(2)}^{\mu}&=\left(0,-h_{\otimes},1+\frac{1}{2}h_{\oplus},0\right),\\\tau_{(3)}^{\mu}&=(0,0,0,1).\end{aligned} \tag{32}$$

Equation (32) indicates that the zeroth and third components of the tetrads coincide completely with the time and z axes in the chosen coordinates, respectively. Furthermore, $\tau_{(1)}^{\mu}$ has only the projection on the x axis; thus $\tau_{(1)}^{\mu}$ actually points at the x axis. This means that the azimuth ϕ in the tetrads and that in the chosen coordinates are the same, while the deviation of $\tau_{(2)}^{\mu}$ from the y axis is only on the order of $h_{\otimes}$.

With the help of Eqs. (3), (4), (27), (28), and (32), neglecting high-order infinitely small quantities, we obtain

$$E_{(x)}=cF_{(01)}=cF_{\mu\nu}\tau^{\mu}_{(0)}\tau^{\nu}_{(1)}$$
$$=\tilde{E}^{(0)}_{x}+\tilde{E}^{(1)}_{x}-\frac{1}{2}h_{xx}\tilde{E}^{(0)}_{x}$$
$$=\psi+\tilde{E}^{(1)}_{x}-\frac{1}{2}h_{\oplus}\psi,$$

$$E_{(y)}=cF_{(02)}=cF_{\mu\nu}\tau^{\mu}_{(0)}\tau^{\nu}_{(2)}=\tilde{E}^{(1)}_{y}-h_{\otimes}\psi,$$

$$E_{(z)}=cF_{(03)}=cF_{\mu\nu}\tau^{\mu}_{(0)}\tau^{\nu}_{(3)}=0,$$

$$B_{(x)}=F_{(32)}=F_{\mu\nu}\tau^{\mu}_{(3)}\tau^{\nu}_{(2)}$$
$$=\tilde{B}^{(1)}_{x}+h_{xy}(\hat{B}^{(0)}_{y}+\tilde{B}^{(0)}_{y})$$
$$=\tilde{B}^{(1)}_{x}+h_{\otimes}\left(\hat{B}^{(0)}_{y}-\frac{i}{\omega_e}\frac{\partial\psi}{\partial z}\right),$$

$$B_{(y)}=F_{(13)}=F_{\mu\nu}\tau^{\mu}_{(1)}\tau^{\nu}_{(3)}$$
$$=\hat{B}^{(0)}_{y}+\tilde{B}^{(0)}_{y}+\tilde{B}^{(1)}_{y}$$
$$=\hat{B}^{(0)}_{y}-\frac{i}{\omega_e}\frac{\partial\psi}{\partial z}+\tilde{B}^{(1)}_{y},$$

$$B_{(z)}=F_{(21)}=F_{\mu\nu}\tau^{\mu}_{(2)}\tau^{\nu}_{(1)}=\tilde{B}^{(0)}_{z}=\frac{i}{\omega_e}\frac{\partial\psi}{\partial y}. \quad (33)$$

As we pointed out above, here $|h\tilde{F}^{(0)}_{\mu\nu}|\sim A\tilde{B}^{(0)}$, $|\tilde{F}^{(1)}_{\mu\nu}|\sim A\hat{B}^{(0)}_{y}$, and in our case, $\hat{B}^{(0)}\sim 10$ T, $\tilde{B}^{(0)}\sim 10^{-3}$ T; thus we have $|h\tilde{F}^{(0)}_{\mu\nu}|/|\tilde{F}^{(1)}_{\mu\nu}|\approx\tilde{B}^{(0)}/\hat{B}^{(0)}_{y}\approx 10^{-4}$, so that the $h\tilde{F}^{(0)}_{\mu\nu}$ terms in Eq. (33) can be neglected again. In this case Eq. (33) can be further reduced to (in region II $-l/2\leqslant z\leqslant l/2$)

$$E_{(x)}=\psi+\tilde{E}^{(1)}_{x}$$
$$=\psi+\frac{i}{2}A_{\oplus}\hat{B}^{(0)}_{y}k_g c(z+l/2)\exp[i(k_g z-\omega_g t)]$$
$$+b_1\exp[i(k_g z-\omega_g t)]$$
$$+c_1\exp[i(k_g z+\omega_g t)],$$

$$B_{(y)}=\hat{B}^{(0)}_{y}-\frac{i}{\omega_e}\frac{\partial\psi}{\partial z}+\tilde{B}^{(1)}_{y}$$
$$=\hat{B}^{(0)}_{y}-\frac{i}{\omega_e}\frac{\partial\psi}{\partial z}+\frac{i}{2}A_{\oplus}\hat{B}^{(0)}_{y}k_g(z+l/2)\exp[i(k_g z-\omega_g t)]+b_2\exp[i(k_g z-\omega_g t)]$$
$$+c_2\exp[i(k_g z+\omega_g t)], \quad (34)$$

$$E_{(y)}=\tilde{E}^{(1)}_{y}$$
$$=-\frac{1}{2}A_{\otimes}\hat{B}^{(0)}_{y}k_g c(z+l/2)\exp[i(k_g z-\omega_g t)]$$
$$+ib_3\exp[i(k_g z-\omega_g t)]+ic_3\exp[i(k_g z+\omega_g t)],$$

$$B_{(x)}=\tilde{B}^{(1)}_{x}+h_{\otimes}\hat{B}^{(0)}_{y}$$
$$=\frac{1}{2}A_{\otimes}\hat{B}^{(0)}_{y}k_g(z+l/2)\exp[i(k_g z-\omega_g t)]$$
$$+ib_4\exp[i(k_g z-\omega_g t)]+ic_4\exp[i(k_g z+\omega_g t)]+iA_{\otimes}\hat{B}^{(0)}_{y}\exp[i(k_g z-\omega_g t)], \quad (35)$$

and

$$E_{(z)}=0,$$
$$B_{(z)}=\tilde{B}^{(0)}_{z}=\frac{i}{\omega_e}\frac{\partial\psi}{\partial y}. \quad (36)$$

C. The particular solutions satisfying boundary conditions

In fact, the perturbative parts in Eqs. (34)–(36) are the general solutions of Eqs. (20)–(25) in region II ($-l/2\leqslant z\leqslant l/2$). We shall define the constants in Eqs. (34) and (35) to give the corresponding particular solutions satisfying the boundary conditions.

Clearly, the perturbative e.m. fields in the regions I, II, and III must satisfy the boundary conditions (the continuity conditions)

$$(\tilde{F}^{(1)}_{(\mu\nu)I})_{z=-l/2}=(\tilde{F}^{(1)}_{(\mu\nu)II})_{z=-l/2},$$
$$(\tilde{F}^{(1)}_{(\mu\nu)II})_{z=l/2}=(\tilde{F}^{(1)}_{(\mu\nu)III})_{z=l/2}. \quad (37)$$

If one chooses the real part of the purely perturbative fields in Eqs. (34) and (35), then we have

$$\tilde{E}^{(1)}_{(x)}=-\frac{1}{2}A_{\oplus}\hat{B}^{(0)}_{y}k_g c(z+l/2)\sin(k_g z-\omega_g t)$$
$$+b_1\cos(k_g z-\omega_g t)+c_1\cos(k_g z+\omega_g t),$$

$$\tilde{B}^{(1)}_{(y)}=-\frac{1}{2}A_{\oplus}\hat{B}^{(0)}_{y}k_g(z+l/2)\sin(k_g z-\omega_g t)$$
$$+b_2\cos(k_g z-\omega_g t)+c_2\cos(k_g z+\omega_g t), \quad (38)$$

$$\tilde{E}^{(1)}_{(y)}=-\frac{1}{2}A_{\otimes}\hat{B}^{(0)}_{y}k_g c(z+l/2)\cos(k_g z-\omega_g t)$$
$$-b_3\sin(k_g z-\omega_g t)-c_3\sin(k_g z+\omega_g t),$$

$$\tilde{B}^{(1)}_{(x)}=\frac{1}{2}A_{\otimes}\hat{B}^{(0)}_{y}k_g(z+l/2)\cos(k_g z-\omega_g t)$$
$$-b_4\sin(k_g z-\omega_g t)-c_4\sin(k_g z+\omega_g t)$$
$$-A_{\otimes}\hat{B}^{(0)}_{y}\sin(k_g z-\omega_g t). \quad (39)$$

A physically reasonable requirement is that there is no the perturbative e.m. wave propagating along the negative z direction in region III ($z\geqslant l/2$). Here we shall consider one

more simple case, i.e., the perturbative e.m. wave in the negative z direction is also absent in region I ($z \leqslant -l/2$). In order to satisfy the boundary conditions Eq. (37) and the above requirement, from Eqs. (29) and (37)–(39), one finds

$$b_1 = -\frac{1}{4}A_{\oplus}\hat{B}_y^{(0)}c, \quad b_2 = \frac{1}{4}A_{\oplus}\hat{B}_y^{(0)}, \quad b_3 = \frac{1}{4}A_{\otimes}\hat{B}_y^{(0)}c,$$

$$b_4 = -\frac{3}{4}A_{\otimes}\hat{B}_y^{(0)},$$

$$c_1 = \frac{1}{4}A_{\oplus}\hat{B}_y^{(0)}c, \quad c_2 = -\frac{1}{4}A_{\oplus}\hat{B}_y^{(0)}, \quad c_3 = \frac{1}{4}A_{\otimes}\hat{B}_y^{(0)}c,$$

$$c_4 = \frac{1}{4}A_{\otimes}\hat{B}_y^{(0)}, \tag{40}$$

and

$$l = n\lambda_g \quad (n \text{ is integer}). \tag{41}$$

In this case we have the perturbative e.m. fields in the above three regions as follows.

(a) Region I ($z \leqslant -l/2, \hat{B}^{(0)} = 0$):

$$\tilde{E}_{(x)}^{(1)} = c\tilde{F}_{(01)}^{(1)} = \tilde{E}_{(y)}^{(1)} = c\tilde{F}_{(02)}^{(1)} = 0,$$

$$\tilde{B}_{(x)}^{(1)} = \tilde{F}_{(32)}^{(1)} = \tilde{B}_{(y)}^{(1)} = \tilde{F}_{(13)}^{(1)} = 0; \tag{42}$$

(b) region II ($-l/2 \leqslant z \leqslant l/2, \hat{B}^{(0)} = \hat{B}_y^{(0)}$):

$$\tilde{E}_{(x)}^{(1)} = -\frac{1}{2}A_{\oplus}\hat{B}_y^{(0)}k_g c\ (z + l/2)\sin(k_g z - \omega_g t) - \frac{1}{2}A_{\oplus}\hat{B}_y^{(0)}c\ \sin(k_g z)\sin(\omega_g t),$$

$$\tilde{B}_{(y)}^{(1)} = -\frac{1}{2}A_{\oplus}\hat{B}_y^{(0)}k_g(z + l/2)\sin(k_g z - \omega_g t) + \frac{1}{2}A_{\oplus}\hat{B}_y^{(0)}\sin(k_g z)\sin(\omega_g t); \tag{43}$$

$$\tilde{E}_{(y)}^{(1)} = -\frac{1}{2}A_{\otimes}\hat{B}_y^{(0)}k_g c(z + l/2)\cos(k_g z - \omega_g t) - \frac{1}{2}A_{\otimes}\hat{B}_y^{(0)}c\ \sin(k_g z)\cos(\omega_g t),$$

$$\tilde{B}_{(x)}^{(1)} = \frac{1}{2}A_{\otimes}\hat{B}_y^{(0)}k_g(z + l/2)\cos(k_g z - \omega_g t) - \frac{1}{2}A_{\otimes}\hat{B}_y^{(0)}\ \sin(k_g z)\cos(\omega_g t); \tag{44}$$

(c) region III ($l/2 \leqslant z \leqslant l_0, \hat{B}^{(0)} = 0$):

$$\tilde{E}_{(x)}^{(1)} = -\frac{1}{2}A_{\oplus}\hat{B}_y^{(0)}k_g c l\ \sin(k_g z - \omega_g t),$$

$$\tilde{B}_{(y)}^{(1)} = -\frac{1}{2}A_{\oplus}\hat{B}_y^{(0)}k_g l\ \sin(k_g z - \omega_g t), \tag{45}$$

$$\tilde{E}_{(y)}^{(1)} = -\frac{1}{2}A_{\otimes}\hat{B}_y^{(0)}k_g c l\ \cos(k_g z - \omega_g t),$$

$$\tilde{B}_{(x)}^{(1)} = \frac{1}{2}A_{\otimes}\hat{B}_y^{(0)}k_g l\ \cos(k_g z - \omega_g t); \tag{46}$$

where l_0 is the size of the effective region in which the second-order perturbative e.m. power fluxes, such as $(1/\mu_0)(\tilde{E}_{(x)}^{(1)}\tilde{B}_{(y)}^{(1)})$, $(1/\mu_0)(\tilde{E}_{(y)}^{(1)}\tilde{B}_{(x)}^{(1)})$, retain a plane wave form. Notice that the power fluxes in region II contain parts with a space accumulation effect, i.e., they depend upon the square of the interaction dimension. This is because the GW's and e.m. waves have the same velocity, so that the two waves can generate an optimum coherent effect in the propagating direction. It is easy to show that, if we choose the imaginary part of the purely perturbative fields in Eqs. (34) and (35), we can obtain similar results, but Eq. (41) will be replaced by

$$l = (2n + 1)\frac{\lambda_g}{2} \quad (n \text{ is an integer}). \tag{47}$$

Logi and Mickelson [29] used Feynman perturbation techniques to analyze the perturbative e.m. waves (photon fluxes) produced by a weak GW (gravitons) passing through a static magnetic (or electrostatic) field, and found that perturbative e.m. waves (photon fluxes) propagate only in the same and in the opposite propagation directions of the GW (gravitons); the latter is weaker than the former or is absent. Obviously, our results and the calculation by Logi and Mickelson are consistent. However, due to the weakness of the interaction of the GW's (gravitons) with the e.m. fields (photons), we shall focus our attention on the first-order perturbative power fluxes produced by the coherent synchroresonance of the above perturbative e.m. fields with the background Gaussian beam, not only the second-order perturbative e.m. power fluxes themselves, such as $(1/\mu_0)(\tilde{E}_{(x)}^{(1)}\tilde{B}_{(y)}^{(1)})$ and $(1/\mu_0)(\tilde{E}_{(y)}^{(1)}\tilde{B}_{(x)}^{(1)})$.

D. The first-order perturbative electromagnetic power fluxes

The generic expression for the energy-momentum tensor of the e.m. fields in GW fields is given by

$$T^{\mu\nu} = \frac{1}{\mu_0}\left(-F_{\alpha}^{\mu}F^{\nu\alpha} + \frac{1}{4}g^{\mu\nu}F_{\alpha\beta}F^{\alpha\beta}\right). \tag{48}$$

Because $F_{\mu\nu} = F_{\mu\nu}^{(0)} + \tilde{F}_{\mu\nu}^{(1)}$ and $|\tilde{F}_{\mu\nu}^{(1)}| \ll |F_{\mu\nu}^{(0)}|$ for nonvanishing $F_{\mu\nu}^{(0)}$ and $\tilde{F}_{\mu\nu}^{(1)}$, $T^{\mu\nu}$ can be decomposed into

$$T^{\mu\nu} = T_{\mu\nu}^{(0)} + T_{\mu\nu}^{(1)} + T_{\mu\nu}^{(2)}, \tag{49}$$

where $\overset{(0)}{T}{}^{\mu\nu}$ is the energy-momentum tensor of the background e.m. field, and $\overset{(1)}{T}{}^{\mu\nu}$ and $\overset{(2)}{T}{}^{\mu\nu}$ represent first-and second-order perturbations to $\overset{(0)}{T}{}^{\mu\nu}$ in the presence of the GW.

Using Eq. (16), $\overset{(0)}{T}{}^{\mu\nu}$, $\overset{(1)}{T}{}^{\mu\nu}$, and $\overset{(2)}{T}{}^{\mu\nu}$ can be written as

$$\overset{(0)}{T}{}^{\mu\nu}=\frac{1}{\mu_0}\left(-F^{\mu(0)}_{\alpha}F^{\nu\alpha(0)}+\frac{1}{4}\eta^{\mu\nu}F^{(0)}_{\alpha\beta}F^{\alpha\beta(0)}\right), \tag{50}$$

$$\overset{(1)}{T}{}^{\mu\nu}=\frac{1}{\mu_0}\left[-(F^{\mu(0)}_{\alpha}\tilde{F}^{\nu\alpha(1)}+\tilde{F}^{\mu(1)}_{\alpha}F^{\nu\alpha(0)})+\frac{1}{4}\eta^{\mu\nu}(\tilde{F}^{(1)}_{\alpha\beta}F^{\alpha\beta(0)}+F^{(0)}_{\alpha\beta}\tilde{F}^{\alpha\beta(1)})-\frac{1}{4}h^{\mu\nu}F^{(0)}_{\alpha\beta}F^{\alpha\beta(0)}\right], \tag{51}$$

$$\overset{(2)}{T}{}^{\mu\nu}=\frac{1}{\mu_0}\left[-\tilde{F}^{\mu(1)}_{\alpha}\tilde{F}^{\nu\alpha(1)}+\frac{1}{4}\eta^{\mu\nu}\tilde{F}^{(1)}_{\alpha\beta}\tilde{F}^{\alpha\beta(1)}-\frac{1}{4}h^{\mu\nu}(F^{(0)}_{\alpha\beta}\tilde{F}^{\alpha\beta(1)}+\tilde{F}^{(1)}_{\alpha\beta}F^{\alpha\beta(0)})\right]. \tag{52}$$

For nonvanishing $\overset{(0)}{T}{}^{\mu\nu}$, $\overset{(1)}{T}{}^{\mu\nu}$, and $\overset{(2)}{T}{}^{\mu\nu}$, we have

$$|\overset{(0)}{T}{}^{\mu\nu}|\gg|\overset{(1)}{T}{}^{\mu\nu}|\gg|\overset{(2)}{T}{}^{\mu\nu}|. \tag{53}$$

Therefore, for the effect of the GW, we are interested in $\overset{(1)}{T}{}^{\mu\nu}$ but not in $\overset{(0)}{T}{}^{\mu\nu}$ and $\overset{(2)}{T}{}^{\mu\nu}$. Nevertheless, it can be shown from Eqs. (1), (3), (5)–(8), (15), (42)–(46) and (52) that the average value of $\overset{(2)}{T}{}^{00}$ with respect to time is always positive. Thus it expresses essentially the net increasing quantity of the energy density of the e.m. fields. In particular, under resonant conditions, it should correspond to the resonant graviton-photon conversion at the quantum level [29–31]. But because $|\overset{(2)}{T}{}^{\mu\nu}|\ll|\overset{(1)}{T}{}^{\mu\nu}|$ for nonvanishing $\overset{(1)}{T}{}^{\mu\nu}$ and $\overset{(2)}{T}{}^{\mu\nu}$, the second-order perturbations are often far below the requirements for an observable effect. In this case it has only theoretical interest. However, for some astrophysical situations, it is possible to cause observable effects, because very large e.m. fields and very strong GW's often occur simultaneously and these fields extend over a very large area [32,33].

By using Eqs. (1), (3), (5)–(8), (15), (42)–(46), and (51), we obtain

$$\overset{(1)}{S}{}^{r}=c\overset{(1)}{T}{}^{01}=\frac{1}{\mu_0}(\tilde{E}^{(1)}_{(\phi)}\tilde{B}^{(0)}_{(z)})=-\frac{1}{\mu_0}(\tilde{E}^{(1)}_{(x)}\tilde{B}^{(0)}_{(z)})\sin\phi+\frac{1}{\mu_0}(\tilde{E}^{(1)}_{(y)}\tilde{B}^{(0)}_{(z)})\cos\phi, \tag{54}$$

$$\overset{(1)}{S}{}^{\phi}=c\overset{(1)}{T}{}^{02}=-\frac{1}{\mu_0}(\tilde{E}^{(1)}_{(r)}\tilde{B}^{(0)}_{(z)})=-\frac{1}{\mu_0}(\tilde{E}^{(1)}_{(x)}\tilde{B}^{(0)}_{(z)})\cos\phi-\frac{1}{\mu_0}(\tilde{E}^{(1)}_{(y)}\tilde{B}^{(0)}_{(z)})\sin\phi, \tag{55}$$

$$\overset{(1)}{S}{}^{z}=c\overset{(1)}{T}{}^{03}=\frac{1}{\mu_0}(\tilde{E}^{(0)}_{(x)}\tilde{B}^{(1)}_{(y)})+\frac{1}{\mu_0}(\tilde{E}^{(1)}_{(x)}\tilde{B}^{(0)}_{(y)}), \tag{56}$$

where $\overset{(1)}{S}{}^{r}$, $\overset{(1)}{S}{}^{\phi}$, and $\overset{(1)}{S}{}^{z}$ represent the first-order radial, tangential, and axial perturbative power flux densities, respectively. As we have shown above, for high-frequency perturbative power fluxes, only their nonvanishing average values with respect to time have an observable effect. It is easily seen from Eqs. (1), (5)–(8), and (42)–(46) that average values of the perturbative power flux densities Eqs. (54)–(56) vanish in the whole frequency range where $\omega_e\neq\omega_g$. In other words, only under the condition of $\omega_e=\omega_g$ (synchroresonance) do $\overset{(1)}{S}{}^{r}$, $\overset{(1)}{S}{}^{\phi}$, and $\overset{(1)}{S}{}^{z}$ have nonvanishing average values with respect to time.

In the following we study only the tangential average power flux density $\langle\overset{(1)}{S}{}^{\phi}\rangle_{\omega_e=\omega_g}$. Introducing Eqs. (1), (8), and (42)–(46) into Eq. (55), and setting $\delta=\pi/2$ in Eq. (1) (this is always possible), we have

$$\langle\overset{(1)}{S}{}^{\phi}\rangle_{\omega_e=\omega_g}=\langle\overset{(1)}{S}{}^{\phi}_{\oplus}\rangle_{\omega_e=\omega_g}+\langle\overset{(1)}{S}{}^{\phi}_{\otimes}\rangle_{\omega_e=\omega_g}, \tag{57}$$

where

$$\langle\overset{(1)}{S}{}^{\phi}_{\oplus}\rangle_{\omega_e=\omega_g}=-\frac{1}{\mu_0}\langle\tilde{E}^{(1)}_{(x)}\tilde{B}^{(0)}_{(z)}\rangle\cos\phi,$$

$$\langle\overset{(1)}{S}{}^{\phi}_{\otimes}\rangle_{\omega_e=\omega_g}=-\frac{1}{\mu_0}\langle\tilde{E}^{(1)}_{(y)}\tilde{B}^{(0)}_{(z)}\rangle\sin\phi. \tag{58}$$

$\langle\overset{(1)}{S}{}^{\phi}_{\oplus}\rangle_{\omega_e=\omega_g}$ and $\langle\overset{(1)}{S}{}^{\phi}_{\otimes}\rangle_{\omega_e=\omega_g}$ represent the average values of the first-order tangential perturbative power flux densities generated by the states of + polarization and × polarization of the GW, Eq. (15), respectively. Using Eqs. (1), (8), (42)–(46), (57), and (58) and the boundary conditions [see Eqs. (37) and (41)], one finds the following.

(a) Region I ($z\leqslant -l/2$),

$$\langle\overset{(1)}{S}{}^{\phi}_{\oplus}\rangle_{\omega_e=\omega_g}=\langle\overset{(1)}{S}{}^{\phi}_{\otimes}\rangle_{\omega_e=\omega_g}=0. \tag{59}$$

(b) Region II ($-l/2\leqslant z\leqslant l/2$),

$$\langle \overset{(1)}{S^{\phi}_{\oplus}} \rangle_{\omega_e=\omega_g} = \left\{ \frac{A_{\oplus}\hat{B}_y^{(0)}\psi_0 k_g r(z+l/2)}{8\mu_0[1+(z/f)^2]^{1/2}(z+f^2/z)} \cos\left(\tan^{-1}\frac{z}{f} - \frac{k_g r^2}{2R} \right) + \frac{A_{\oplus}\hat{B}_y^{(0)}\psi_0 r(z+l/2)}{4\mu_0 W_0^2[1+(z/f)^2]^{3/2}} \sin\left(\tan^{-1}\frac{z}{f} - \frac{k_g r^2}{2R} \right) \right.$$
$$- \frac{A_{\oplus}\hat{B}_y^{(0)}\psi_0 r}{8\mu_0[1+(z/f)^2]^{1/2}(z+f^2/z)} \sin(k_g z) \cos\left(\tan^{-1}\frac{z}{f} - \frac{k_g r^2}{2R} - k_g z \right) - \frac{A_{\oplus}\hat{B}_y^{(0)}\psi_0 r}{4\mu_0 k_g W_0^2[1+(z/f)^2]^{3/2}} \sin(k_g z)$$
$$\left. \times \sin\left(\tan^{-1}\frac{z}{f} - \frac{k_g r^2}{2R} - k_g z \right) \right\} \exp\left(-\frac{r^2}{W^2} \right) \sin(2\phi), \tag{60}$$

$$\langle \overset{(1)}{S^{\phi}_{\otimes}} \rangle_{\omega_e=\omega_g} = \left\{ \frac{A_{\otimes}\hat{B}_y^{(0)}\psi_0 k_g r(z+l/2)}{4\mu_0[1+(z/f)^2]^{1/2}(z+f^2/z)} \sin\left(\frac{k_g r^2}{2R} - \tan^{-1}\frac{z}{f} \right) + \frac{A_{\otimes}\hat{B}_y^{(0)}\psi_0 r(z+l/2)}{2\mu_0 W_0^2[1+(z/f)^2]^{3/2}} \cos\left(\frac{k_g r^2}{2R} - \tan^{-1}\frac{z}{f} \right) \right.$$
$$+ \frac{A_{\otimes}\hat{B}_y^{(0)}\psi_0 r}{4\mu_0[1+(z/f)^2]^{1/2}(z+f^2/z)} \sin(k_g z) \sin\left(k_g z - \tan^{-1}\frac{z}{f} + \frac{k_g r^2}{2R} \right) + \frac{A_{\otimes}\hat{B}_y^{(0)}\psi_0 r}{2\mu_0 k_g W_0^2[1+(z/f)^2]^{3/2}} \sin(k_g z)$$
$$\left. \times \cos\left(k_g z - \tan^{-1}\frac{z}{f} + \frac{k_g r^2}{2R} \right) \right\} \exp\left(-\frac{r^2}{W^2} \right) \sin^2\phi. \tag{61}$$

(c) Region III ($l/2 \leqslant z \leqslant l_0$),

$$\langle \overset{(1)}{S^{\phi}_{\oplus}} \rangle_{\omega_e=\omega_g} = \left\{ \frac{A_{\oplus}\hat{B}_y^{(0)}\psi_0 k_g l r}{8\mu_0[1+(z/f)^2]^{1/2}(z+f^2/z)} \cos\left(\tan^{-1}\frac{z}{f} - \frac{k_g r^2}{2R} \right) + \frac{A_{\oplus}\hat{B}_y^{(0)}\psi_0 l r}{4\mu_0 W_0^2[1+(z/f)^2]^{3/2}} \sin\left(\tan^{-1}\frac{z}{f} - \frac{k_g r^2}{2R} \right) \right\}$$
$$\times \exp\left(-\frac{r^2}{W^2} \right) \sin(2\phi), \tag{62}$$

$$\langle \overset{(1)}{S^{\phi}_{\otimes}} \rangle_{\omega_e=\omega_g} = \left\{ \frac{A_{\otimes}\hat{B}_y^{(0)}\psi_0 k_g l r}{4\mu_0[1+(z/f)^2]^{1/2}(z+f^2/z)} \sin\left(\frac{k_g r^2}{2R} - \tan^{-1}\frac{z}{f} \right) + \frac{A_{\otimes}\hat{B}_y^{(0)}\psi_0 l r}{2\mu_0 W_0^2[1+(z/f)^2]^{3/2}} \cos\left(\frac{k_g r^2}{2R} - \tan^{-1}\frac{z}{f} \right) \right\}$$
$$\times \exp\left(-\frac{r^2}{W^2} \right) \sin^2\phi. \tag{63}$$

It is easily shown that the nonvanishing first-order perturbative power flux densities are much greater than corresponding second-order perturbative power flux densities. The quantum picture of this process can be described as the interaction of the photons with the gravitons in a background of virtual photons (or virtual gravitons) as a ''catalyst'' [29,34], which can greatly increase the interaction cross section between the photons and gravitons. In other words the interaction may effectively change the physical behavior (e.g., propagation direction, distribution, polarization, and phase) of the photons in the local regions; even if the net increase of the photon number (the e.m. energy) of the entire e.m. system approaches zero, such properties may be very useful to display very weak signals of GW's.

Equations (60)–(63) show that because there are nonvanishing $\overset{(1)}{S^{\phi}_{\oplus}}$ (which depend on the + polarization state of the GW) and $\overset{(1)}{S^{\phi}_{\otimes}}$ (which depend on the × polarization state of the GW), the first-order tangential perturbative power fluxes are expressed as a ''left circular wave'' and a ''right circular wave'' in cylindrical polar coordinates around the symmetrical axis of the Gaussian beam, but $\langle \overset{(1)}{S^{\phi}_{\oplus}} \rangle_{\omega_e=\omega_g}$ and $\langle \overset{(1)}{S^{\phi}_{\otimes}} \rangle_{\omega_e=\omega_g}$ have a different physical behavior. By comparing Eqs. (60)–(63) with Eqs. (9)–(11), we can see the following. (a) $\langle \overset{(1)}{S^{\phi}_{\oplus}} \rangle_{\omega_e=\omega_g}$ and $\langle \overset{(0)}{S^{\phi}} \rangle$ have the same angular distribution factor $\sin(2\phi)$, thus $\langle \overset{(1)}{S^{\phi}_{\oplus}} \rangle_{\omega_e=\omega_g}$ will be swamped by the background power flux $\langle \overset{(0)}{S^{\phi}} \rangle$; namely, in this case $\langle \overset{(1)}{S^{\phi}_{\oplus}} \rangle_{\omega_e=\omega_g}$ has no observable effect. (b) The angular distribution factor of $\langle \overset{(1)}{S^{\phi}_{\otimes}} \rangle_{\omega_e=\omega_g}$ is $\sin^2\phi$; it is different from that of $\langle \overset{(0)}{S^{\phi}} \rangle$. Therefore, $\langle \overset{(1)}{S^{\phi}_{\otimes}} \rangle_{\omega_e=\omega_g}$, in principle, has an observable effect. In particular, at the surfaces $\phi = \pi/2, 3\pi/2$, $\langle \overset{(0)}{S^{\phi}} \rangle \equiv 0$, while $|\langle \overset{(1)}{S^{\phi}_{\otimes}} \rangle_{\omega_e=\omega_g}| = |\langle \overset{(1)}{S^{\phi}_{\otimes}} \rangle_{\omega_e=\omega_g}|_{\max}$; this is satisfactory (although

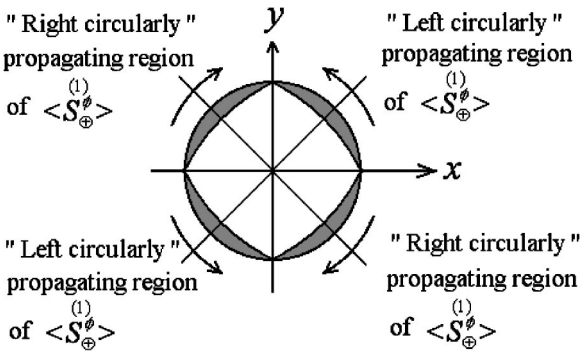

FIG. 2. Distribution of $\langle S^{(1)\phi}_{\oplus}\rangle_{\omega_e=\omega_g}$ at the plane $z=l/2=n/2\lambda_g$ (n is integer) in the cylindrical polar coordinates. It has maxima at $\phi=\pi/4$, $3\pi/4$, $5\pi/4$, and $7\pi/4$, while it vanishes at $\phi=0$, $\pi/2$, π and $3\pi/2$. Here $l=0.1$ m, $\lambda_g=0.01$ m and $r=0.05$ m, and the GW propagates along the z axis.

$\langle S^{(0)r}\rangle$ and $\langle S^{(1)\phi}_{\otimes}\rangle_{\omega_e=\omega_g}$ have the same angular distribution factor $\sin^2\phi$, the propagation direction of $\langle S^{(0)r}\rangle$ is perpendicular to that of $\langle S^{(1)\phi}_{\otimes}\rangle_{\omega_e=\omega_g}$; thus $\langle S^{(0)r}\rangle$ (including $\langle S^{(0)z}\rangle$) has no essential contribution in the purely tangential direction).

Figure 2 gives the distribution of $\langle S^{(1)\phi}_{\oplus}\rangle_{\omega_e=\omega_g}$ on the plane $z=l/2=n/2\lambda_g$ (n is an integer) in cylindrical polar coordinates, while Fig. 3 gives the distribution of $\langle S^{(1)\phi}_{\otimes}\rangle_{\omega_e=\omega_g}$ in the plane $z=0$ in cylindrical polar coordinates.

From Eqs. (10), (11), (60), and (61), we can also see that $\langle S^{(0)r}\rangle=\langle S^{(0)\phi}\rangle=\langle S^{(1)\phi}_{\oplus}\rangle_{\omega_e=\omega_g}\equiv 0$ in the plane $z=0$, while

$$\langle S^{(1)\phi}_{\otimes}\rangle_{\omega_e=\omega_g}=\frac{A_{\otimes}\hat{B}^{(0)}_y\psi_0 lr}{4\mu_0 W_0^2}\exp\left(-\frac{r^2}{W_0^2}\right)\sin^2\phi. \qquad (64)$$

In Table I we list the distribution of $\langle S^{(0)\phi}\rangle$, $\langle S^{(1)\phi}_{\oplus}\rangle_{\omega_e=\omega_g}$, and $\langle S^{(1)\phi}_{\otimes}\rangle_{\omega_e=\omega_g}$ in some typical regions. Table I, Eqs. (60)–(63), and Figs. 2 and 3 show that the plane $z=0$ and the planes $\phi=\pi/2,3\pi/2$ are the three most interesting regions. For the former, $\langle S^{(0)\phi}\rangle=\langle S^{(0)r}\rangle=\langle S^{(1)\phi}_{\oplus}\rangle_{\omega_e=\omega_g}\equiv 0$, but a nonvanishing $\langle S^{(1)\phi}_{\otimes}\rangle_{\omega_e=\omega_g}$ exists; for the latter two, $\langle S^{(0)\phi}\rangle=\langle S^{(0)\phi}_{\oplus}\rangle_{\omega_e=\omega_g}\equiv 0$, but there is a nonzero $\langle S^{(1)\phi}_{\otimes}\rangle_{\omega_e=\omega_g}$. This means that any nonvanishing tangential e.m. power flux in such regions will express the pure electromagnetic-gravitational perturbation.

E. Numerical estimations

If we describe the perturbation in the quantum language (photon flux), the corresponding perturbative photon flux n_ϕ caused by $\langle S^{(1)\phi}_{\otimes}\rangle_{\omega_e=\omega_g}$ in the plane $\phi=\pi/2$ (we note that

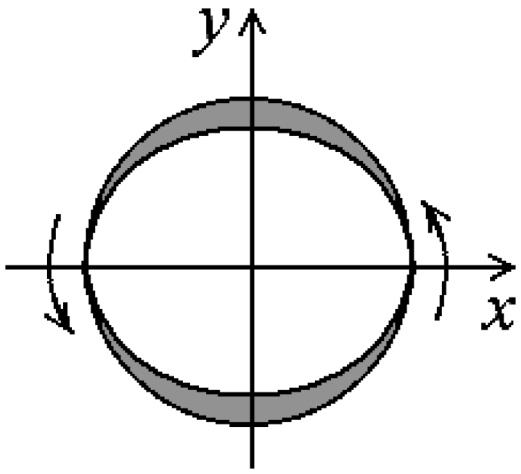

FIG. 3. Distribution of $\langle S^{(1)\phi}_{\otimes}\rangle_{\omega_e=\omega_g}$ in the plane $z=0$ in cylindrical polar coordinates, It has maxima at $\phi=\pi/2$ and $3\pi/2$, while it vanishes at $\phi=0,\pi$. Unlike Fig. 2, $\langle S^{(1)\phi}_{\otimes}\rangle_{\omega_e=\omega_g}$ at the $z=0$ is completely "left-hand circular." Here $r=0.05$ m, $\lambda_g=0.01$ m, and the GW propagates along the z axis.

$\langle S^{(1)\phi}_{\otimes}\rangle_{\omega_e=\omega_g}$ is the unique nonvanishing power flux density passing through the plane) is given by

$$n_\phi=\frac{\langle u^{(1)\phi}_{\otimes}\rangle_{\omega_e=\omega_g,\phi=\pi/2}}{\hbar\omega_e}=\frac{1}{\hbar\omega_e}\int_0^{W_0}\int_{-l/2}^{l_0}\langle S^{(1)\phi}_{\otimes}\rangle_{\omega_e=\omega_g,\phi=\pi/2}dzdr, \qquad (65)$$

where $\langle u^{(1)\phi}_{\otimes}\rangle_{\omega_e=\omega_g,\phi=\pi/2}=\int_0^{W_0}\int_{-l/2}^{l_0}\langle S^{(1)\phi}_{\otimes}\rangle_{\omega_e=\omega_g,\phi=\pi/2}dzdr$ is the total perturbative power flux passing through the plane $\phi=\pi/2$ and $\hbar$ is the Planck constant.

In order to give reasonable estimations, we choose achievable values of the e.m. parameters in the present experiments. (1) $\psi_0=3\times10^5$ V m^{-1} (i.e., $\psi_0/c=10^{-3}$ T), the amplitude of the Gaussian beam. If the spot radius W_0 of the Gaussian beam is limited to 0.05 m, the corresponding power can be estimated as $P=\int_0^{W_0}\langle S^{(0)z}\rangle_{z=0}2\pi rdr\approx10^5$ W [see Eq. (9)]; this power is well within the reach of current technology [21,35]. For the Gaussian beam with $\nu_e=3\times10^{10}$ Hz, this is equivalent to a photon flux $n^{(0)}$ of 5×10^{27} s^{-1} roughly. (2) $\hat{B}^{(0)}_y=30$ T, the strength of the background static magnetic field; this is the achievable strength of a stationary magnetic field under present experimental conditions [36]. (3) $A_{\otimes}=10^{-30}$, $\omega_g/2\pi=\nu_g=3\times10^{10}$ Hz, these are the typical orders of magnitude expected quintessential inflationary models [1]. Substituting Eqs. (61), (63), and the above parameters into Eq. (65), and setting $W_0=0.05$ m, $l=0.1$ m, $l_0=0.3$ m, we obtain $n_\phi\approx1.57\times10^3$ s^{-1} (see Table II). Up to now, this is the largest perturbative photon flux in a series of results [7–9]. Recently, we analyzed and estimated them under typical labo-

TABLE I. The distribution of $\overset{(0)}{\langle S^{\phi}\rangle}$, $\overset{(1)}{\langle S^{\phi}_{\oplus}\rangle}_{\omega_e=\omega_g}$, and $\overset{(1)}{\langle S^{\phi}_{\otimes}\rangle}_{\omega_e=\omega_g}$ in some typical regions.

	Angular distribution factor	Plane $z=0$	Planes $\phi=\pi/4,5\pi/4$	Planes $\phi=3\pi/4,7\pi/4$	Planes $\phi=\pi/2,3\pi/2$
$\overset{(0)}{\langle S^{\phi}\rangle}$	$\sin(2\phi)$	0	$\lvert\overset{(0)}{\langle S^{\phi}\rangle}\rvert=\lvert\overset{(0)}{\langle S^{\phi}\rangle}\rvert_{max}$, "left circular" propagation	$\lvert\overset{(0)}{\langle S^{\phi}\rangle}\rvert=\lvert\overset{(0)}{\langle S^{\phi}\rangle}\rvert_{max}$, "right circular" propagation	0
$\overset{(1)}{\langle S^{\phi}_{\oplus}\rangle}_{\omega_e=\omega_g}$	$\sin(2\phi)$	0	$\lvert\overset{(1)}{\langle S^{\phi}_{\oplus}\rangle}_{\omega_e=\omega_g}\rvert=\lvert\overset{(1)}{\langle S^{\phi}_{\oplus}\rangle}_{\omega_e=\omega_g}\rvert_{max}$, "left circular" propagation	$\lvert\overset{(1)}{\langle S^{\phi}_{\oplus}\rangle}_{\omega_e=\omega_g}\rvert=\lvert\overset{(1)}{\langle S^{\phi}_{\oplus}\rangle}_{\omega_e=\omega_g}\rvert_{max}$, "right circular" propagation	0
$\overset{(1)}{\langle S^{\phi}_{\otimes}\rangle}_{\omega_e=\omega_g}$	$\sin^2\phi$	$\lvert\overset{(1)}{\langle S^{\phi}_{\otimes}\rangle}_{\omega_e=\omega_g}\rvert$ $=\lvert\overset{(1)}{\langle S^{\phi}_{\otimes}\rangle}_{\omega_e=\omega_g}\rvert_{max}$ at $\phi=\pi/2,3\pi/2$	There are nonvanishing values; "left circular" propagation	There are nonvanishing values; "left circular" propagation	$\lvert\overset{(1)}{\langle S^{\phi}_{\otimes}\rangle}_{\omega_e=\omega_g}\rvert$ $=\lvert\overset{(1)}{\langle S^{\phi}_{\otimes}\rangle}_{\omega_e=\omega_g}\rvert_{max}$, "left circular" propagation

ratory parameter conditions. If the integration region of the radial coordinate r in Eq. (65) is moved to $W_0 \leqslant r \leqslant r_0$ (here $W_0=0.05$ m, $r_0=0.1$ m), in the same way, the corresponding perturbative photon flux n'_{ϕ} can be estimated as $n'_{\phi}=(1/\hbar\omega_e)\int_{W_0}^{r_0}\int_{-l/2}^{l_0}\overset{(1)}{\langle S^{\phi}_{\otimes}\rangle}_{\omega_e=\omega_g,\phi=\pi/2}dzdr = 0.96\times10^3\ \mathrm{s}^{-1}\approx10^3\ \mathrm{s}^{-1}$. Although then $n'_{\phi}<n_{\phi}$, it retains basically the order of $10^3\ \mathrm{s}^{-1}$, and because the "receiving" plane of the tangential perturbative photon flux has already moved to the region outside the spot radius W_0 of the Gaussian beam, it has a more realistic meaning to distinguish and display the perturbative photon flux.

Figure 4 gives the rating curve between $\overset{(1)}{\langle S^{\phi}_{\otimes}\rangle}_{\omega_e=\omega_g}$ and $\overset{(0)}{\langle S^{z}\rangle}$ in the plane $z=0$; here r is the radial coordinate.

Figure 5 gives the rating curve between n_{ϕ} and the axis coordinate z, and the relative parameters are chosen as $\nu_e=\nu_g=\omega_g/2\pi=3\times10^{10}$ Hz, $A_{\otimes}=10^{-30}$, $\hat{B}_y^{(0)}=30$ T, $\psi_0=3\times10^5$ V m^{-1}, $l=0.1$ m, $l_0=0.3$ m, and $W_0=0.05$ m. Figure 5 shows that n_{ϕ} has a good space accumulation effect as z increases. In fact, in addition to the third and fourth terms in Eq. (61), the rest in the expression for $\overset{(1)}{\langle S^{\phi}_{\otimes}\rangle}_{\omega_e=\omega_g}$, Eq. (61) and Eq. (63), is all a slow enough variational function in the z direction. This means that the value of $\overset{(1)}{\langle S^{\phi}_{\otimes}\rangle}_{\omega_e=\omega_g}$ is slowly variational and keeps its sign invariant in the whole region of the coherent resonance (here it is about the region of $80\lambda_g$, namely, 0.8 m); thus $\overset{(1)}{\langle S^{\phi}_{\otimes}\rangle}_{\omega_e=\omega_g}$ are "left circularly" propagated from $-l/2$ to l_0.

Table II gives the tangential perturbative photon fluxes and corresponding relevant parameters in three cases. In the first case $W_{01}=0.05$ m, in the second case $W_{02}=0.02$ m, in the third case $W_{03}=0.1$ m, but the background Gaussian beam has the same power in the three cases, i.e., $P\approx10^5$ W. Because $W_{03}>W_{01}>W_{02}$, $\psi_{03}<\psi_{01}<\psi_{02}$. Table II shows that the tangential perturbation in the Gaussian beam with larger W_0 (i.e., smaller θ) has a better physical effect than that in the Gaussian beam with smaller W_0 (i.e., larger θ); here θ is the spreading angle of the beam, $\theta=\tan^{-1}(\lambda_e/\pi W_0)\approx\lambda_e/\pi W_0$.

We emphasize that here $n_{\phi}\propto\psi_0\propto\sqrt{P}$ [see Eqs. (61), (63), and (65); P is the power of the Gaussian beam], and at the same time $n_{\phi}\propto\hat{B}_y^{(0)}$. Therefore, if P is reduced to 10^3 W, then $n_{\phi}\approx1.57\times10^2\ \mathrm{s}^{-1}$; and even if P is reduced to 10 W

TABLE II. The tangential perturbative photon fluxes and corresponding relevant parameters.

A	ν_g (Hz)	W_0 (m)	θ	$\overset{(1)}{\langle u^{\phi}_{\otimes}\rangle}_{\omega_e=\omega_g}$(W)	n_{ϕ} (s^{-1})
10^{-30}	3×10^{10}	0.05	6.36×10^{-2}	3.11×10^{-20}	1.57×10^3
10^{-30}	3×10^{10}	0.02	15.78×10^{-2}	1.31×10^{-20}	6.61×10^2
10^{-30}	3×10^{10}	0.10	3.18×10^{-2}	3.14×10^{-20}	1.58×10^3

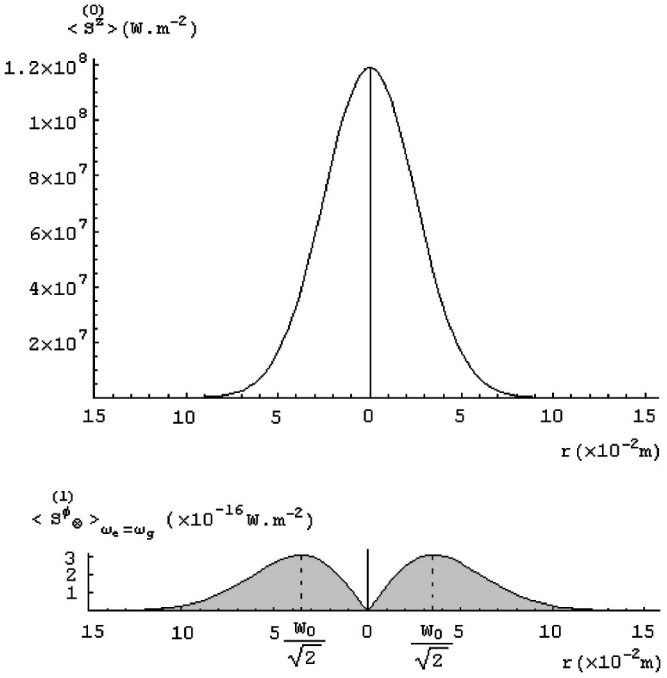

FIG. 4. Rating curve between $\langle S^{(1)\phi}_{\otimes}\rangle_{\omega_e=\omega_g}$ and $\langle S^{(0)z}\rangle$ in the plane $z=0$; here r is the radial coordinate and $\phi=\pi/2$ or $3\pi/2$ in Eq. (64). It shows that $|\langle S^{(1)\phi}_{\otimes}\rangle_{\omega_e=\omega_g}|=|\langle S^{(1)\phi}_{\otimes}\rangle_{\omega_e=\omega_g}|_{max}$ at $r=W_0/\sqrt{2}$. The background axial power flux density $\langle S^{(0)z}\rangle$ is a typical Gaussian distribution, and $|\langle S^{(0)z}\rangle|\gg|\langle S^{(1)\phi}_{\otimes}\rangle_{\omega_e=\omega_g}|_{max}$. However, because the propagatoin direction of $\langle S^{(0)z}\rangle$ is perpendicular to that of $\langle S^{(1)\phi}_{\otimes}\rangle_{\omega_e=\omega_g}$, $\langle S^{(0)z}\rangle$ has no contribution in the purely tangential direction. The shaded part expresses $\langle S^{(1)\phi}_{\otimes}\rangle_{\omega_e=\omega_g}$. Here $\nu_e=\nu_g=\omega_g/2\pi=3\times10^{10}$ Hz, $A_{\otimes}=10^{-30}$, $\hat{B}^{(0)}_y=30$ T, $\psi_0=3\times10^5$ V m^{-1}, $l=0.1$ m, and $W_0=0.05$ m.

(this is already a very relaxed requirement), we still have $n_\phi\approx1.57\times10$ s^{-1}. Thus, if possible, increasing $\hat{B}^{(0)}_y$ (in this way the number of the background real photons does not change) has a better physical effect than increasing P. According to the above discussion, we give some values for the power P of the background Gaussian beam and corresponding parameters n_ϕ and n'_ϕ (see Table III).

In particular, since n'_ϕ indicates the tangential perturbative photon flux passing through the "receiving" plane $\phi=\pi/2$ ($\sim10^{-2}$ m^2) outside the spot radius W_0 of the Gaussian beam, the results provided a more realistic test scheme.

IV. GEOMETRICAL PHASE SHIFT PRODUCED BY HIGH-FREQUENCY RELIC GRAVITATIONAL WAVES

Mitskievich and Nesterov [37] investigated the Berry's phase shift of a monochromatic e.m. wave beam in a plane monochromatic GW field, and it was shown that (a) for parallel propagating GW and e.m. wave, the phase shift is absent; (b) when the waves are mutually orthogonal, a nonvanishing phase shift will be produced, and the phase shift is

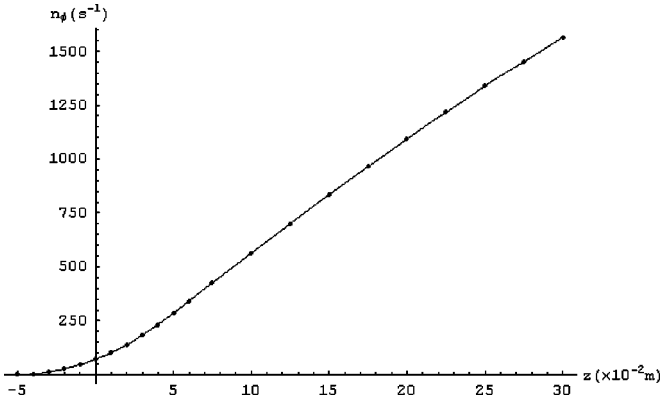

FIG. 5. Rating curve between n_ϕ and the axial coordinate z, here $\nu_e=\nu_g=\omega_g/2\pi=3\times10^{10}$ Hz, $A_{\otimes}=10^{-30}$, $\hat{B}^{(0)}_y=30$ T, $\psi_0=3\times10^5$ V m^{-1}, and $W_0=0.05$ m. It shows that the purely tangential perturbative photon flux passing through the plane $\phi=\pi/2$ with $10^{-2}m^2$ would be expected to be 1.57×10^3 s^{-1}.

proportional to the distance propagated by the e.m. wave [see Eq. (6) in Ref. [37]], i.e.,

$$\Delta\alpha=A(\Lambda-\sin\Lambda)\sin(\Lambda+\delta'), \tag{66}$$

Here,

$$\Lambda=2\pi L/\lambda_g=\frac{L}{c}\omega_g, \tag{67}$$

A is the amplitude of the GW (e.g., $A_\oplus$ or $A_\otimes$), L is the distance between the observer and the reflecting system of the e.m. wave, and $\lambda_e=\lambda_g,\omega_e=\omega_g$; L is also the interaction dimension of the GW with the e.m. wave. If $\Lambda\gg1$, from Eq. (66), we have

$$\Delta\alpha\approx A\Lambda\ \sin(\Lambda+\delta'), \tag{68}$$

namely, one obtains a linear increase of the phase shift. Equations (67) and (68) show that a large distance L and high frequency ω_g will produce a better physical effect than that of a small L and low frequency ω_g.

As we have pointed out, unlike an ideal plane monochromatic e.m. wave, the Gaussian beam is a realized e.m. wave beam satisfying physical boundary conditions, and we shall show that for a Gaussian beam with a small spreading angle, the wave beam in the region near the symmetrical axis can be approximately seen as a quasiplane wave. In this case it is possible to estimate the geometrical phase shift in the Gaussian beam.

TABLE III. The power of the background Gaussian beam and corresponding n_ϕ and n'_ϕ.

P (W)	n_ϕ (s^{-1})	n'_ϕ (s^{-1})
10^5	$\sim1.57\times10^3$	$\sim10^3$
10^3	$\sim1.57\times10^2$	$\sim10^2$
10	$\sim1.57\times10$	~10

TABLE IV. The geometrical phase shift produced by GW's in e.m. wave beams with the same frequencies.

	A	$\nu_g=\nu_e$ (Hz)	Waveform	Interaction dimension L (m)	Λ	Geometrical phase shift $\Delta\alpha$
(a)	10^{-22}	3×10^{3}	Monochromatic plane e.m. wave	3.8×10^{8} (cislunar distance)	2.4×10^{4}	2.4×10^{-18}
(b)	10^{-30}	3×10^{10}	Gaussian beam	1	2.5×10^{2}	2.5×10^{-28}
(c)	10^{-30}	3×10^{10}	Gaussian beam	38	2.4×10^{4}	2.4×10^{-26}
(d)	10^{-30}	3×10^{10}	Gaussian beam	5×10^{9} (LISA dimension)	3.1×10^{12}	3.1×10^{-18}

In order to simplify our analysis, we consider only the real part of Eq. (1). From Eq. (1) we have

$$\mathrm{Re}(\psi)=f_1(r,z)\cos(k_e z-\omega_e t)+f_2(r,z)\sin(k_e z-\omega_e t), \tag{69}$$

where

$$f_1(r,z)=\frac{\psi_0}{[1+(z/f)^2]^{1/2}}\exp\left(-\frac{r^2}{W^2}\right)\times\cos\left(\tan^{-1}\frac{z}{f}-\frac{k_g r^2}{2R}-\delta\right), \tag{70}$$

$$f_2(r,z)=\frac{\psi_0}{[1+(z/f)^2]^{1/2}}\exp\left(-\frac{r^2}{W^2}\right)\times\sin\left(\tan^{-1}\frac{z}{f}-\frac{k_g r^2}{2R}-\delta\right). \tag{71}$$

Equations (69)–(71) show that for a Gaussian beam with a small spreading angle, the deviation of the propagation direction from the z axis in the region near the axis would be very small, and for the high-frequency band, the functions f_1 and f_2, Eqs. (70) and (71), will be slowly variational functions in the z direction. In this case, the change of the Gaussian beam in space-time mainly depends on the propagation factors $\cos(k_e z-\omega_e t)$ and $\sin(k_e z-\omega_e t)$. In this sense it is just characteristic of the plane wave. Therefore, for a GW propagating along the y axis, because its propagation direction is perpendicular to the z axis, it would generate a phase shift satisfying approximately Eq. (66) or Eq. (68). Notice that, since in this case the propagation direction of the GW is parallel with the static magnetic field $\hat{B}_y^{(0)}$, whether from the classical or the quantum theory of weak fields, the GW (gravitons) does not produce perturbative e.m. fields (photon fluxes) in static magnetic fields [28,29]. Thus all the first-order perturbations expressed as Eqs. (54)–(56) vanish.

It is interesting to compare the geometrical phase shift produced by the high-frequency relic GW of $\nu_g=3\times10^{10}$ Hz and $A=10^{-30}$ in a Gaussian beam with the phase shift generated by the expected astronomical GW of $\nu_g=3\times10^{3}$ Hz and $A=10^{-22}$ in a plane monochromatic e.m. wave (see Table IV). With the help of Eqs. (66)–(68), we list some typical parameters in Table IV.

We can see from Table IV that scheme (a)has the typical parameters of the expected astronomical GW's [see the analysis in Ref. [37] and Eqs. (60)–(68)], and $\Lambda=2.5\times10^{4}$, $\Delta\alpha=2.4\times10^{-18}$. This means that in this case a GW of $A=10^{-22}$ and $\nu_g=10^{3}$ Hz can be treated as an effective magnitude of some 10^{-18}, but it needs an interaction dimension of cislunar distance (i.e., the reflecting system of the e.m. wave beam is placed on the surface of the moon). For scheme (d), the phase shift may achieve the same order of magnitude as in scheme (a), but it needs the interacting dimension of LISA ($\sim10^{9}$ m), and it is necessary to construct a very strong Gaussian beam with a small spreading angle in the microwave frequency band for LISA. This seems to be beyond the ability of presently conceived technology. Nevertheless, if the amplitude of the high-frequency relic GW ($\nu_g\sim10^{10}$ Hz) and the amplitude of the expected astronomical GW ($\nu_g\sim10^{3}$ Hz) have the same order of magnitude, then the geometrical phase shift $\Delta\alpha$ produced by the former will be seven orders of magnitude larger than that generated by the latter.

V. CONCLUDING REMARKS

(1) For the relic GW's predicted by quintessential inflationary models, since a large amount of the energy of the GW's may be stored around the GHz band, using smaller e.m. systems (e.g., microwave cavities or the Gaussian beam discussed in this paper) for detection purposes seems plausible. In particular, the Gaussian beams can be considered as new possible candidates. For high-frequency relic GW's with typical order of $\nu_g=10^{10}$ Hz, $h=10^{-30}$ in the models, under the condition of resonant response, the corresponding first-order perturbative photon flux passing through the region 10^{-2} m would be expected to be 10^{3} s^{-1}. This is the largest perturbative photon flux we have recently analyzed and estimated using typical laboratory parameters.

(2) In our e.m. system, the perturbative effects produced by the $+$ and $\times$ polarization states of the high-frequency relic GW have different physical behavior. In particular, since the first-order tangential perturbative photon flux produced by the $\times$ polarization state of the relic GW is perpendicular to the background photon fluxes, it will be a unique nonvanishing photon flux passing through some special planes. Therefore any photon measured from such a photon flux in the above special planes may be a signal of e.m. perturbation produced by the GW; this property may be

promising to further improve the e.m. response to the GW.

(3) As for the geometrical phase shift produced by the high-frequency relic GW, because of the excessive small amplitude of the relic GW, the phase shift is still below the requirement for experimental observation. Thus the outlook for such schemes may not be promising unless there are stronger high-frequency relic GW's. But for the dimensions of LISA (of course, in this case it needs a very strong microwave beam), it is possible to get an observable effect.

The relic GW's are quite possibly the few windows from which we can look back at the early history of our Universe, while the high-frequency relic GW's in the GHz band predicted by quintessential inflationary models can possibly provide a new criterion to distinguish between the quintessential inflationary and the ordinary inflationary models. As pointed out by Ostriker and Sternhardt [5], whatever the origin of quintessence, its dynamism could solve the thorny problem of fine-tuning our Universe. If we could display the signal of the high-frequency relic GW's in the quintessential inflationary models through the e.m. response or other means, it would not only provide incontrovertible evidence of the GW and quintessence, but also give us an extraordinary opportunity to look back at the early Universe. Therefore, if there is even a small chance that the signal of the high-frequency relic GW's is detectable, then it is worth pursuing.

ACKNOWLEDGMENTS

One of the authors (F.Y.L.) would like to thank J. D. Fan, Y. M. Malozovsky, W. Johnson, and E. Daw for very useful discussions and suggestions. This work is supported by the National Nature Science Foundation of China under Grants No. 10175095 and No. 19835040 and by the Foundation of Gravitational and Quantum Laboratory of Hupeh Province under Grant No. GQ0101.

APPENDIX A: THE CAVITY ELECTROMAGNETIC RESPONSE TO GRAVITATIONAL WAVES

For the cavity electromagnetic response to GW's, the best detection state is the resonant response of the fundamental e.m. normal modes of the cavity to the GW's, since in this case it is possible to generate the maximal e.m. perturbation. For resonant states (whether the background e.m. field stored inside the cavity is only a static field or both the static magnetic field and the normal modes), the display condition at the level of a quantum nondemolition measurement can be written as [10,11]

$$\frac{(hQ)^2B^2V}{\mu_0\hbar\omega_e}\geqslant 1, \tag{A1}$$

where Q is the quality factor of the cavity, V is its volume, and B is the background static magnetic field. In order to satisfy the fundamental resonant condition, the estimated cavity dimensions should be comparable to the wavelength of the GW. However, the dimensions cannot be too big. This is because constructing a superconducting cavity with typical dimension $l\geqslant 100$ m may be unrealistic under the present experimental conditions. The low-frequency nature of the usual astronomical GW's seems to greatly limit the perturbative effects in the cavity's fundamental e.m. normal modes. For the high-frequency GW's in the GHz band, the corresponding resonant condition can be relaxed, but the cavity size cannot be excessively small, even if the condition $l\geqslant\lambda_g$ can be satisfied, since in this case the cavity cannot store enough e.m. energy to generate an observable perturbation. If GW's detected by the cavity have excessively high frequency, e.g., $\nu_g=\nu_e>10^9$ Hz, we can see from Eq. (A1) that the requirements for the other parameters will be a big challenge. For instance, if one hopes to detect a high-frequency relic GW with $h=10^{-30}$ and $\nu_g=10^9$ Hz in quintessential inflationary models, we need $Q=10^{12}$, $B=30$ T and $V=100$ m^3 at least; then the corresponding signal accumulation time will be $\tau\approx Q/\omega_e\approx 10^3$ s. If $h=10^{-30}$, $\nu_g=10^8$ Hz, we need $Q=10^{12}$, $B=30$ T and $V=10$ m^3 (i.e., the typical dimension of the cavity will be $l\sim 2.2$ m) at least, then $\tau\approx Q/\omega_e\approx 10^4$ s. Increasing the quality factor Q and using squeezed quantum states may be a promising direction [11]. For the former, the requirements on the other parameters can be further relaxed; for the latter, the signal accumulation time could be decreased. Therefore, for the fundamental resonant response, a suitable size of the cavity may be of the magnitude of a meter, the corresponding resonant frequency band should be 10^8 Hz$<\nu_g<10^9$ Hz roughly [the region (4)-2 in Fig. 1]. In order to detect GW's of 10^8 Hz $<\nu_g<10^9$ Hz, the thermal noise must be $kT<h\nu_g$ which corresponds to $T\leqslant 10^{-3}$ K (see Appendix D).

Moreover, the resonant difference-frequency schemes suggested in Refs. [38,39] can be used as e.m. detectors for high-frequency GW's. The detector consists of two identical high-frequency cavities (e.g., two coupled spherical cavities as discussed in the recent paper [39]). When the GW frequency ν_g equals the frequency difference $|\nu_1-\nu_2|$ of the two cavity modes (i.e., $\nu_g=|\nu_1-\nu_2|$, and ν_1, $\nu_2\gg\nu_g$), then the detector can get maximal e.m. energy transfer. Following [39] we learn that the sensitivity of the e.m. detector would be expected to be $\delta h\sim 10^{-20}-10^{-22}$ for GW's in the 10^3-10^4 Hz frequency band [the region (4)-1 in Fig. 1]. If this e.m. detector is advanced, it might detect GW's in the GHz band. Reference [40] reported an e.m. detection scheme for high-frequency GW's by the interaction between a GW and the polarization vector of an e.m. wave in repeated circuits of a closed loop. In this scheme, because of the linearly cumulative effect of the rotation of the polarization vector of the e.m. wave, the expected sensitivity can reach up to $\delta h\sim 10^{-18}-10^{-19}$ for GW's of 10^8-10^9 Hz [the region (4)-2 in Fig. 1]. The above two schemes [39,40] are both sensitive to the polarization of the incoming GW signal. Although the sensitivity of the above e.m. detectors is still below the requirements for an observable effect of the high-frequency relic GW's, advanced e.m. detector schemes would be promising.

APPENDIX B: THE DIMENSIONLESS AMPLITUDE h AND THE POWER SPECTRUM S_h OF THE HIGH-FREQUENCY RELIC GRAVITATIONAL WAVES

The relation between the logarithmic energy spectrum Ω_{GW} and the power spectrum S_h of the relic GW given by

Ref. [1] [see Eq. (A18) in Ref. [1]] is

$$\Omega_{GW}(\nu,\eta_0)=\frac{4\pi^2}{3H_0^2}\nu_g^3 S_h(\nu,\eta_0), \tag{B1}$$

where H_0 is the present value of the Hubble constant, i.e., $H_0=3.24\times10^{-18}\ \mathrm{s}^{-1}$. From Eq. (B1), one finds [1]

$$S_h(\nu,\eta_0)\approx 8\times10^{-37}\Omega_{GW}(\nu,\eta_0)\frac{(\mathrm{Hz})^2}{\nu_g^3}. \tag{B2}$$

In the peak region of the logarithmic energy spectrum of the relic GW in the quintessential inflationary models, $\Omega_{GW}\approx 5\times10^{-6}$ [1]. Thus, for the relic GW of $\nu_g=10^9$ Hz, we have $S_h\approx 4\times10^{-69}$ s; for the relic GW of $\nu_g=10^{10}$ Hz, one finds $S_h\approx 4\times10^{-72}$ s.

For continuous GW's, the dimensionless amplitude h can be estimated roughly as

$$h\approx(S_h\Delta\nu_g)^{1/2}, \tag{B3}$$

where $\Delta\nu_g$ is the corresponding bandwidth. According to the estimation in Ref. [1] (see Fig. 2 in Ref. [1] or Fig. 1 in this paper), the bandwidth in the high-frequency peak region is about $\Delta\nu_g\approx10^{11}$–$10^9$ Hz$\approx10^{11}$ Hz. Thus, from Eq. (B3), we have

$$\begin{aligned} &h\approx10^{-29}\text{–}10^{-30}\ (\text{for the relic GW of } \nu_g=10^9\ \mathrm{Hz}),\\ &h\approx10^{-30}\text{–}10^{-31}\ (\text{for the relic GW of } \nu_g=10^{10}\mathrm{Hz}). \end{aligned} \tag{B4}$$

The above results and orders of magnitude estimated in Ref. [1] are basically consistent. In this paper we have chosen $h\sim10^{-30}$. Of course, these estimations are only approximate average effects. In fact, because of the uncertainty of some relative cosmological parameters [1,2] in certain regions, it is possible to cause small deviations to the above estimations.

APPENDIX C: MINIASTRODYNAMICAL SPACE TEST OF RELATIVITY USING OPTICAL DEVICES (MINI-ASTROD)

Mini-ASTROD is a new cooperative project (China, Germany, etc.) [26]. The basic scheme of the mini-ASTROD is to use two-way laser interferometric ranging and laser pulse ranging between the mini-ASTROD spacecraft in the solar system and deep space laser stations on Earth to improve the precision of solar-system dynamics, solar-system constants, and ephemera, to measure relativistic gravity effects, to test the fundamental laws of space-time more precisely, to improve the measurement of the time rate of change of the gravitational constant, and to detect low-frequency GW's ($\sim10^{-6}$–10^{-3} Hz).

The follow-up scheme of the mini-ASTROD is ASTROD [41], i.e., the mini-ASTROD is a down-scaled version of the ASTROD. Both LISA and mini-ASTROD are all space detection projects, but there are some differences in their study objectives; the detection frequency band of the GW's for the mini-ASTROD will be moved to 10^{-6} Hz (see Fig. 1). With optical methods, the mini-ASTROD should achieve the same sensitivity as LISA [26]. Thus, the mini-ASTROD [26], ASTROD [41], and LISA have a certain complementarity.

APPENDIX D: NOISE PROBLEMS

The noise problems of e.m. detection systems have been extensively discussed and reviewed [1,10,35,38,39]; here we will give only a brief review of problems relevant to the e.m. detection of high-frequency GW's (especially the e.m. response of a Gaussian beam).

The thermal noise is one of the fundamental sources of limitation of the detection sensitivity [38,39]. Unlike in the usual mechanical detectors, the frequencies of the e.m. systems resonant with the high-frequency GW's in the GHz band are often much higher than those of the usual environment noise (e.g., mechanical, seismic, and others). Thus e.m. detection systems are easier to shield from external e.m. noise (e.g., using Faraday cages) than are mechanical detection systems from mechanical vibration. For the e.m. response of microwave cavities to high-frequency GW's, the noise problem can be more conveniently treated by considering the relevant quantum character [35]. For a superconducting cavity at a temperature $T=T_0$, if the background e.m. field is only a static magnetic or static electric field, the display condition can be given by Eq. (A1), while then the cavity vacuum contains thermal photons with an energy spectrum given by the Plank formula:

$$u_\nu(\nu)=\frac{8\pi\nu^2}{c^3}\frac{h\nu}{\exp(h\nu/KT_0)-1}, \tag{D1}$$

where u_ν and ν are the energy density and the photon frequency, respectively, while k is the Boltzmann constant. If the cavity is cooled down to $T_0=1$ mK, according to the Wien law, the energy density has a maximum at $\nu_m=5.87\times10^7$ Hz (i.e., $\lambda_m\approx3$ m; the corresponding photon density is about $10^{-8}\ \mathrm{cm}^{-3}$). For the perturbative photons produced by high-frequency GW's of $\nu_g=3\times10^9$ Hz under resonant conditions, we have $\nu_e=\nu_g$ (i.e., $\lambda=0.1$ m), which is higher than ν_m (i.e., $\nu_e\approx30\nu_m$). Therefore, the crucial parameter for the thermal noise is the selected frequency and not the total background photon number; namely, in this case, the thermal noise can be effectively suppressed as long as the detector can select the right frequency.

For the e.m. response of a Gaussian beam in the high-frequency region of $\nu_e=\nu_g=3\times10^{10}$ Hz, because the frequencies of the usual environmental noise are much lower than ν_e, it cannot have an essential influence on the perturbative photon flux; while for possible external e.m. noise sources, using a Faraday cage would be very useful. Once the e.m. system (the Gaussian beam and the static magnetic field) is isolated from the outside world by the Faraday cage, possible noise sources would be the remaining thermal photons and self-background action. However, because of the ''random motion'' of the remaining thermal photons and the specific distribution of the photon fluxes in the e.m. system (as we discussed earlier), the influence of such noise on the

highly ''directional'' propagated perturbative photon fluxes would be effectively suppressed in the local regions. Therefore, the key parameters for the noise problems are the selected perturbative photon fluxes (e.g., n_ϕ and n'_ϕ) passing through special planes (e.g., planes $\phi=\pi/2$ and $3\pi/2$) and not all the background photons. Moreover, low-temperature vacuum operation might effectively reduce the frequency of the remaining thermal photons and avoid dielectric dissipation. If the frequency ν_m of the remaining thermal photons is much lower than that of the perturbative photon fluxes, i.e., $\nu_m \ll \nu_e$, then the above two kinds of photons will be more easily distinguished.

[1] M. Giovannini, Phys. Rev. D **60**, 123511 (1999).
[2] M. Giovannini, Class. Quantum Grav. **16**, 2905 (1999).
[3] P. Peebles and A. Vilenkin, Phys. Rev. D **59**, 063505 (1999).
[4] A. Riazuelo and J. P. Uzan, Phys. Rev. D **62**, 083506 (2000).
[5] J. P. Ostriker and P. J. Sternhardt, Sci. Am. (Int. Ed.) **284**, 46 (2001).
[6] L. Mang *et al.*, Astrophys. J. **530**, 17 (2000).
[7] F. Y. Li and M. X. Tang, Chin. Phys. Lett. **16**, 12 (1999).
[8] F. Y. Li, M. X. Tang, J. Luo, and Y. C. Li, Phys. Rev. D **62**, 044018 (2000).
[9] F. Y. Li and M. X. Tang, Chin. Phys. **11**, 461 (2002).
[10] L. P. Grishchuk and M. V. Sazhin, Zh. Éksp. Teor. Fiz. **68**, 1569 (1975) [Sov. Phys. JETP **41**, 787 (1975)].
[11] L. P. Grishchuk and M. V. Sazhin, Zh. Éksp. Teor. Fiz. **84**. 1937 (1983) [Sov. Phys. JETP **53**, 1128 (1983)].
[12] F. Y. Li and M. X. Tang, Int. J. Mod. Phys. D **11**, 1049 (2002).
[13] C. Bradaschia *et al.*, Nucl. Instrum. Methods Phys. Res. A **289**, 518 (1990).
[14] A. Abramovici *et al.*, Science **256**, 325 (1992).
[15] R. Caldwell, M. Kamionkowski, and L. Madley, Phys. Rev. D **59**, 027101 (1999).
[16] Y. Jafry, J. Corneliss, and R. Reinhard, ESA Bull. **18**, 219 (1994).
[17] J. M. Codina, J. Graells, and C. Martín, Phys. Rev. D **21**, 2731 (1980).
[18] A. Modena *et al.*, Nature (London) **377**, 606 (1995).
[19] G. A. Mourou *et al.*, Phys. Today **51**(1), 22 (1998).
[20] B. A. Remington *et al.*, Science **284**, 1488 (1999).
[21] M. Kushwah *et al.*, in IEEE/Symposium on Fusion Engineering 2002, pp. 84–87.
[22] A. Yariv, *Quantum Electronics*, 2nd ed. (Wiley, New York, 1975).
[23] E. Mauceli *et al.*, gr-qc/0007023; M. P. Mchugh *et al.*, Int. J. Mod. Phys. D **9**, 229 (2000).
[24] P. Astone, G. V. Pallottino, and G. Pozzella, Class. Quantum Grav. **14**, 2019 (1997).
[25] M. Cerdonio *et al.*, Class. Quantum Grav. **14**, 1491 (1997).
[26] W. T. Ni *et al.*, Int. J. Mod. Phys. D **11**, 1035 (2002).
[27] L. P. Grishchuk, gr-qc/0002035.
[28] D. Boccaletti, V. De. Sabbata, and P. Fortini, Nuovo Cimento B **70**, 129 (1970).
[29] W. K. Logi and A. R. Mickelson, Phys. Rev. D **16**, 2915 (1977).
[30] P. Chen, ''Resonant Photon-Graviton Conversion in e.m. Fields: From Earth to Heaven,'' Stanford Linear Accelerator Center Report No. PUB-6666, 1994.
[31] H. N. Long, D. V. Soa, and T. A. Tuan, Phys. Lett. A **186**, 382 (1994).
[32] P. Chen, Phys. Rev. Lett. **74**, 634 (1995).
[33] M. Marklund, G. Brodin, and P. Dunsby, Astrophys. J. **536**, 875 (2000).
[34] V. De Sabbata, D. Boccaletti, and C. Gualdi, Sov. J. Nucl. Phys. **8**, 537 (1969).
[35] P. Chen, G. D. Palazzi, K. J. Kim and C. Pellegeini, in *Workshop on Beam-Beam and Beam-Radiation: High Intensity and Nonlinear Effects, Los Angeles, California, 1991*, edited by C. Pellegrini *et al.* (World Scientific, Singapore, 1992), p. 84.
[36] G. Boebinger, A. Passner, and J. Bevk, Sci. Am. (Int. Ed.) **272**, 34 (1995).
[37] N. V. Mitskievich and A. I. Nesterov, Gen. Relativ. Gravit. **27**, 361 (1995).
[38] F. Pegoraro, L. A. Radicati, Ph. Bernard, and E. Picasso, Phys. Lett. **68A**, 165 (1978); E. Iacopini, E. Picasso, F. Pegoraro, and L. A. Radicati, *ibid.* **73A**, 140 (1979).
[39] Ph. Bernard *et al.*, gr-qc/0203024.
[40] A. M. Cruise, Class. Quantum Grav. **17**, 2525 (2000).
[41] W. T. Ni, Int. J. Mod. Phys. D **11**, 947 (2002); A. Rudiger, *ibid.* **11**, 963 (2002).